

TOPICAL REVIEW

Recent advances in III-Sb nanowires: from synthesis to applications

To cite this article: SenPo Yip *et al* 2019 *Nanotechnology* **30** 202003

View the [article online](#) for updates and enhancements.




IOP | ebooksTM

Bringing you innovative digital publishing with leading voices to create your essential collection of books in STEM research.

Start exploring the **collection** - **download the first chapter of every title for free.**

Topical Review

Recent advances in III-Sb nanowires: from synthesis to applications

SenPo Yip^{1,2}, Lifan Shen^{1,3} and Johnny C Ho^{1,2,4,5} ¹ Department of Materials Science and Engineering, City University of Hong Kong, Hong Kong Special Administrative Region of China, People's Republic of China² Shenzhen Research Institute, City University of Hong Kong, Shenzhen 518057, People's Republic of China³ College of Microelectronics and Key Laboratory of Optoelectronics Technology, Faculty of Information Technology, Beijing University of Technology, Beijing 100124, People's Republic of China⁴ State Key Laboratory of Terahertz and Millimeter Waves, City University of Hong Kong, Hong Kong Special Administrative Region of China, People's Republic of China⁵ Centre of Functional Photonics, City University of Hong Kong, Hong Kong Special Administrative Region of China, People's Republic of ChinaE-mail: johnnyho@cityu.edu

Received 31 October 2018, revised 27 November 2018

Accepted for publication 9 January 2019

Published 13 March 2019



Abstract

The excellent properties of III–V semiconductors make them intriguing candidates for next-generation electronics and optoelectronics. Their nanowire (NW) counterparts further provide interesting geometry and a quantum confinement effect which benefits various applications. Among the many members of all the III–V semiconductors, III-antimonide NWs have attracted significant research interest due to their narrow, direct bandgap and high carrier mobility. However, due to the difficulty of NW fabrication, the development of III-antimonide NWs and their corresponding applications are always a step behind the other III–V semiconductors. Until recent years, because of advances in understanding and fabrication techniques, electronic and optoelectronic devices based on III-antimonide NWs with novel performance have been fabricated. In this review, we will focus on the development of the synthesis of III-antimonide NWs using different techniques and strategies for fine-tuning the crystal structure and composition as well as fabricating their corresponding heterostructures. With such development, the recent progress in the applications of III-antimonide NWs in electronics and optoelectronics is also surveyed. All these discussions provide valuable guidelines for the design of III-antimonide NWs for next-generation device utilization.

Keywords: III-antimonide, nanowire, synthesis, electronics, optoelectronics

(Some figures may appear in colour only in the online journal)

1. Introduction

Nowadays, the semiconductor industry is mostly a Si-based industry since the electronics integrated into personal computers and smartphones are largely Si-based devices. However, as the physical limit of the Si-based transistor is approaching, the search for a replacement is fueled up.

Among the different groups of potential replacements, III–V materials are considered a prime candidate and an alternative to replace Si in semiconductor industries owing to them having a direct bandgap and higher bulk carrier mobility than Si.

In particular, semiconductors based on III-antimonide (III-Sb, including GaSb and InSb) and their alloys with other

Table 1. Physical properties of III-Sb semiconductors with reference to Si and other common III–V semiconductors. Si is the indirect bandgap. Data from: <http://ioffe.ru/SVA/NSM/Semicond>.

	InSb	GaSb	Si	GaAs	InAs	InP
Lattice constant (Å)	6.479	6.096	5.431	5.653	6.058	5.869
Bandgap at 300 K (eV)	0.17	0.726	1.12	1.424	0.354	1.344
Electron mobility (cm ² /Vs)	77 000	3000	1400	8500	25 000	5400
Hole mobility (cm ² /Vs)	850	1000	450	400	500	200

III–V materials (e.g. InAs, InP and GaAs) are an interesting group that has attracted a tremendous amount of research interest. This group of materials has a large lattice constant (over 6 Å), a narrow and direct bandgap, high bulk electron and hole mobilities as well as a high g-factor. There are numerous applications of these semiconductors consisting of high-speed, low-power electronics for data processing, infrared (IR) optoelectronics for light emission or sensing and many others [1–3].

At the same time, their nanowire (NW) counterparts provide extra benefits for many advanced utilizations. Generally, NW is a type of structure with a high-aspect ratio in length and diameter. As compared to its bulk counterparts, the advantages of NW include its better stress relaxation when growing heterostructure; its capability of advanced gate stacking integration for nanoscale transistors; its more efficient light adsorption and trapping (in NW arrays) for light sensing, and also its larger area-to-volume ratio for high-performance sensors. Owing to the narrow direct bandgap, III-Sb NW is also capable of being integrated into IR optoelectronics. Importantly, InSb NWs have been uniquely reported as a platform to study Majorana zero modes (MZMs) which benefits our knowledge of condensed-matter physics and might help to realize spin-based quantum computation [4].

Despite having such intriguing properties and potential applications, however, as compared to III-arsenide (III-As) and III-phosphide (III-P), progress in studying III-Sb falls behind substantially. For example, the controllable growth of its pure wurtzite (WZ) phase in NW has only been realized recently. Since then, the development of fabricating III-Sb NWs and their heterostructures has attracted more interest due to a deeper understanding of the growth mechanism and advance in fabrication techniques.

The purpose of this review is to give a general overview of the challenges of growing III-Sb NWs, as well as review the recent progress on III-Sb NW fabrication and some benchmark applications. We will first introduce the physical properties of different III-Sb semiconductors and the recent research focus of their NW format. After that, the effect of Sb atoms in fabricating III-Sb NWs is also discussed. More importantly, the recent research progress including the phase and shape control in growing III-Sb NWs is surveyed. Finally, the electronic and optoelectronic applications utilizing these III-Sb NWs are presented. We end with an outlook on their future research and development directions.

1.1. Physical properties and recent research trend of III-Sb NWs and their heterostructures

In this section, the physical properties of some popular III-Sb alloy NWs and their recent progress are introduced. Their applications are outlined in detail in the Applications section below. Some physical properties of bulk III-Sb are listed in table 1 with comparison to Si, InAs, GaAs and InP.

1.1.1. Binary III-Sb NWs. Binary III-Sb, InSb (6.49 Å), GaSb (6.1 Å) and AlSb (6.13 Å) all have a large lattice constant (all over 6.1 Å). Due to their excellent properties, they have been extensively researched in their bulk form for various applications like electronics, IR detectors, IR lasers and thermophotovoltaic cells [1, 5, 6].

Among the III-Sb materials, InSb and GaSb are the two most researched systems. InSb has the highest bulk electron mobility (78 000 cm² V^{−1} s^{−1}), narrowest direct bandgap (0.17 eV) and largest electron g-factor (51) of the binary III–V semiconductors. With these superior properties, InSb NW can be utilized in high-performance low-power electronics, IR detectors and gas detectors [7]. It is also used in thermoelectric applications due to its high thermoelectric figure of merit [8]. In recent years, a large part of research interest on InSb NW has been focused on developing low dimensional quantum devices for Majorana fermions detection and manipulation as well as developing spin-based quantum computation [4].

On the other hand, GaSb (0.72 eV) is also a direct bandgap material. With such a bandgap, GaSb can be used as a photodetector of the mid-IR spectrum. Also, GaSb is a III–V semiconductor with a high hole mobility among the III–V semiconductors (over 1000 cm² V^{−1} s^{−1}) [9] which makes it a potential building block for a high-performance, p-type transistor for next-generation complementary metal-oxide-semiconductor (CMOS). The GaSb/InAs axial NW heterostructure is frequently used to develop tunnel field-effect transistors (TFETs) which can work below the thermionic limit of 60 mV/decade [10].

Compared with InSb and GaSb, AlSb has a larger but indirect bandgap (1.74 eV) in its zinc-blend (ZB) form. The lattice constant of AlSb is close to InAs (6.06 Å, the lattice mismatch is 1.2%), which has a large conduction band offset (about 1.35 eV) and forms a type II alignment. Therefore, InAs/AlSb was frequently fabricated as a deep quantum well structure for various studies [11, 12]. The study of directly growing AlSb NW is rare. On the other hand, there are

several reports on the InAs/AlSb core-shell NW heterostructure that study the growth behavior as well as the application for photodetectors [13–15].

1.1.2. Ternary and quaternary III-Sb NWs. Apart from the binary III-Sb, the ternary and quaternary alloys are receiving a lot of research interest. The driving force in studying the growth of a ternary and quaternary system is to realize the properties' tunability by precisely controlling the amount of incorporation of other group III (In, Ga and Al) and group V (As and P) elements. The ternary III-Sb alloys cover a large portion of the IR spectrum which makes them attractive candidates for optoelectronics and photodetectors from the near-IR to the far-IR range. Also, their excellent electrical properties and other unique properties make them capable of electronic applications. Here, three relatively more studied ternary III-Sb NWs are introduced. InAsSb NW is the alloy form of two low bandgap III-V materials, InSb and InAs (0.34 eV). One of the interesting properties of InAsSb is that its bandgap can be lower than its constituted III-V materials by adjusting the Sb incorporation. A bandgap as low as 145 meV (at 0 K) can be obtained by tuning the composition (where $x = 0.63$) which is the narrowest direct bandgap among the III-V semiconductors and reaches to the far-IR region. Probing by terahertz and Raman spectroscopy, the electron mobility of InAsSb NW increases with the Sb incorporation, and the mobility of $\text{InAs}_{0.65}\text{Sb}_{0.35}$ NWs exceeds $16\,000\text{ cm}^2\text{ V}^{-1}\text{ s}^{-1}$ at 10 K [16]. Another more studied ternary III-Sb alloy is GaAsSb whose bandgap covers the wavelength range from near-IR (GaAs, 870 nm) to mid-IR (GaSb, 1700 nm) which is important for applications like solar cells, photonics, optical telecommunication, and optoelectronics. GaInSb has been used to fabricate a high-performance p-type transistor and shows good hole mobility [17]. It is considered a promising candidate for next-generation p-channel materials in CMOS technology [2]. The growth behavior of GaInSb NWs on a InSb/InAs wire-on-wire stem and GaSb stem are studied [18, 19]. Other ternary III-Sb alloys are also studied for their growth behavior and unique applications. The growth behavior of InPSb [20, 21] and GaSbP [22] NWs are also studied but have not been much followed up.

There are some reports studying the quaternary III-Sb NWs [23, 24] but overall the research is still in its infancy. The study of quaternary III-Sb NWs is, however, still important for various applications due to it providing more room for the properties engineering.

1.1.3. Heterostructure. One important objective of studying III-Sb NWs is to create a heterostructure. The large lattice misfit between III-Sb materials and a traditional substrate like Si makes it difficult to grow a defectless epitaxial layer without a thick buffer layer, especially when creating heterostructure of InSb and other III-V materials as it has the largest lattice parameter (6.49 Å). The binary III-V semiconductor with the closest lattice parameter is AlSb (6.13 Å) which still has a large lattice mismatch. In bulk form,

a large lattice match creates threading dislocations in the interface which may degrade the transport and optical properties [25, 26].

Fabricating an axial heterostructure is especially important for III-Sb NWs as they usually are hard to nucleate directly on the substrate due to the existence of Sb in the growth environment; the contact angle of the catalytic particle is decreased and might be below the threshold for stable NW growth [27]. Although III-Sb NWs can be grown directly on different crystalline III-V (111)B substrates [27], growing the III-Sb NWs on a stem (usually InAs, InP and GaAs NW) increases the NWs' yield effectively. Generally, InSb NW and its related alloy are grown on a InAs or InP stem [28] while GaSb NW and its related alloy are grown on an InAs and GaAs stem [29].

Another motivation for growing a III-Sb heterostructure is to passivate the surface. III-V NWs usually have a surface layer that consists of a charge-rich layer. This surface layer degrades the device performance and needs to be passivated. Creating a core-shell structure stabilizes the surface dangling bond and isolates the surface of the core from the environment.

Finally, the heterostructure enhances the functionality of the NW. By careful design of the composition of the junctions, the band alignment of the heterostructure can be engineered accordingly. Heterostructures of NW are integrated for different applications like a NW-based light emitter (LED and laser), waveguide, TFET, solar cell and thermoelectric. For example, an InAs/GaSb-based axial p-n junction was used to fabricate a state-of-the-art TFET [30]. Mid-IR lasing was investigated in a GaAsSb-based axial NW structure [31]. An InAs/InSb axial NW was used to fabricate a THz detector [32].

2. Methods fabricating III-Sb NWs

In this part, different mechanisms used to grow III-Sb NWs are presented. Different growth mechanisms have their benefits and disadvantages. Foreign metal-seeded growth, self-seeded, selective-area epitaxy (SAE) and top-down methods are discussed here. In the first three mechanisms, majorly vapor(source)-to-solid (NW) based techniques like chemical vapor deposition (CVD), metalorganic vapor-phase epitaxy (MOVPE) and molecular beam epitaxy (MBE) are presented. However, various approaches like electrodeposition have also been reported to fabricate InSb NWs [33, 34]. Some related recent progress is introduced here as well.

2.1. Foreign metal-seeded growth

Growing NWs using foreign metal nanoparticles as catalysts is a commonly studied method. In this method, absorbing the group III elements of the predetermined NW to the catalytic nanoparticle, the group III element will form an alloy with the metal catalyst. As the supersaturation of the alloyed nanoparticle approaches, the solid phase NW precipitates at the triple interface between the catalytic nanoparticle, growth substrate and the gas (or liquid) phase environment. With this method, the structures of the NW can be guided by a combination of growth

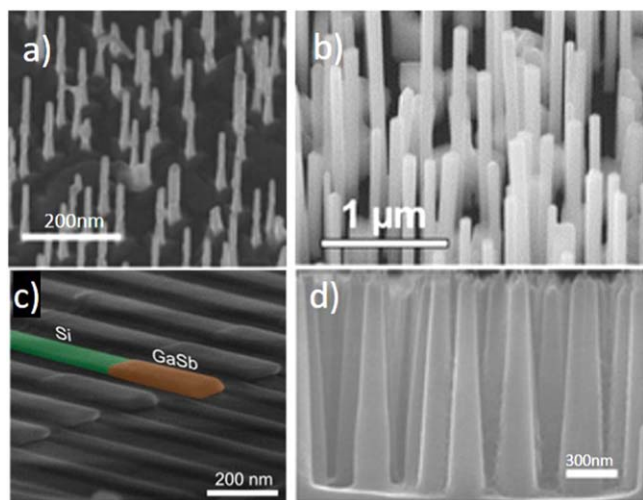


Figure 1. Representative examples of III-Sb fabricated in a different growth mode. (a) Foreign metal-seeded growth: GaAs-GaSb NW grown by a Sn catalyst [42] (reproduced from [42]. © IOP Publishing Ltd. All rights reserved). (b) Self-seeded growth: self-catalyzed $\text{InAs}_{1-x}\text{Sb}_x$ NWs [47] (adapted with permission from [47]. Copyright 2014 American Chemical Society). (c) Selective-area growth (SAG): GaSb NW-like structure grown by template-assisted selective epitaxy (TASE) [62] (adapted with permission from [62]. Copyright 2017 American Chemical Society). (d) Top-down: GaSb NWs fabricated by a self-masked top-down technique [70] (adapted with permission from [70]. Copyright 2015 American Chemical Society).

conditions like temperature, V/III ratio and substrate orientations. Other than these conditions, the choice of catalyst, the alloy composition, and the phase and size of the catalyst also play a significant part [35–39]. Depending on how the source is supplied and the interaction between the source and the catalytic particle, the catalytic growth mechanisms can be categorized as vapor-liquid-solid (VLS), vapor-solid-solid (VSS) and solution-liquid-solid (SLS).

Gold is the most frequently used catalyst due to its low eutectic temperature alloying with other metal elements. For III–V semiconductors, group III elements like Al, Ga and In form homogenous alloys with Au. The majority of reports on the foreign metal-seeded growth of III-Sb NWs are based on a Au nanoparticle either by dewetting of the thin Au film or by direct deposition of the pre-synthesis Au nanoparticle on top of the substrate. One known disadvantage of using Au as the catalyst is the formation of deep-level traps with silicon and degradation of the device performance which makes it forbidden in the CMOS fabrication process [40]. Searching for alternatives to replace Au as a NW catalyst is recommended. However, the use of Au catalyst is still dominant in NW research.

Various metals apart from Au have been used to fabricate III-Sb NWs. For example, Ag, Al, Cu, Ni and Ti were used but some of these have a similar problem to gold or have other issues [41]. In recent years, a research group from Lund used Sn—a group IV element that does not form a mid-gap trap with Si and is frequently used as a dopant for the III–V semiconductor—to fabricate GaSb and GaSb/GaAs axial heterojunctions (figure 1(a)) and study their growth behavior,

structural properties and optical properties [42, 43]. In another report, Yang *et al* used Pd, another Si-based fabrication process-compatible element [41], to fabricate GaSb NWs via a VSS mechanism [44]. The Pd catalysts form a rod-like structure with Ga and guide the NW to grow in a $\langle 111 \rangle$ direction within a narrow diameter range despite growing on amorphous SiO_2 . The p-type transistors fabricated by the obtained GaSb NW show good hole mobility [44]. Those studies might pave the way for CMOS process-compatible foreign metal-seeded III-Sb NW growth.

2.2. Self-seeded growth

This mechanism is very similar to foreign metal-seeded growth regarding using a metal nanoparticle as a catalyst. However, instead of using a foreign metal, this mechanism uses the very element that constitutes the NW itself which is the low melting point group III metal, In or Ga, to grow the III–V NWs. Using the constituent to catalyze the NW growth, this mechanism ensures high chemical purity and is expected to be CMOS compatible. To initiate self-catalyzed NW growth, the creation of Ga or In droplets is necessary before the growth. Also, as the droplet itself might consume during the growth, careful design of a growth parameter is necessary to balance the consumption and accumulation of the group III tip. One of the disadvantages of this method is the difficulty in controlling the position and dimension.

This technique has been used to grow both binary and ternary III-Sb NWs. Self-seeded InSb and GaSb NWs were fabricated on a quartz substrate [45] and various III–V (111)B substrates [46]. Recently, the growth of ternary III-Sb by self-seeded growth has also been demonstrated in InAsSb (figure 1(b)) [47, 48], GaAsSb [49] and InPSb [20, 21]. Creation of III-Sb-based axial and radial heterostructures has also been realized [29, 50, 51], as well as relatively complex heterostructures like InAs/GaSb axial NW which requires switching both group III and group V elements during the NW growth [29]. The capability of creating heterostructures is extremely important as direct nucleation of III-Sb NWs on silicon is difficult and usually requires an InAs, InP or GaAs stem for nucleation.

As knowledge of growing III-Sb NWs has increased drastically in recent years, apart from just growing the NWs, researchers are capable of manipulating the crystal structure of self-seeded III-Sb NWs. For example, self-seeded growth InAs(Sb) NW can be used to create L-shape hierarchical structures by manipulating the In droplet [52].

2.3. SAG

SAG epitaxy is also a self-catalyzed NW growing mechanism. In SAG, a dielectric layer (like Si_xN_y and SiO_2) is first deposited on the crystalline growth substrate. After that, well-defined openings are patterned by e-beam lithography or another lithography-based technique followed by etching on the Si_xN_y or SiO_2 layer. The NW nucleates on the exposed area of a single crystalline substrate grown by SAG in a layer-by-layer mode, and the opening of a mask limits the lateral

growth of the NW. In this sense, the crystal orientation of the substrate determines the NW growth direction of the NWs. During the growth, a catalytic droplet might be involved. Various III-Sb vertical NWs have been reported to be fabricated by SAG especially for the ternary alloy [53–57].

Lateral InSb and GaSb NWs can also be fabricated using a SAG mode on a patterned GaAs(001) substrate with the aid of a hydrogen flux using MBE developed by the Wallart group [58–60]. In-plane GaSb NW structure has been grown directly on a patterned GaAs(001) substrate. The opening has a size of 100 nm and the resultant structure is used to grow in-plane InAs NWs [58, 59]. The in-plane InSb NWs can be fabricated into a more complex planar structure like branched NW by controlling the opening shape [60].

There is a CMOS-compatible technique worth noting that guided the NW epitaxial growth laterally which is called template-assisted selective epitaxy (TASE) developed in IBM [61]. TASE does not require a predeposited catalytic droplet and the NW grows directly on a single crystalline silicon opening. In TASE, the NWs are nucleated on a small Si window in a predefined hollow channel made by SiO₂. The hollow channel defines the dimension and shape of the NWs. Also, antiphase defects and threading dislocations are avoided in this method. So far, high-quality GaSb NWs (figure 1(c)) have been grown by this method which will be discussed in a later part [62].

2.4. Top-down

Fabricating NWs in a top-down manner involves using an etching technique to remove part of the materials. Some would consider the top-down method as a less favorable method for NW fabrication because, during the process, the surface of the NW may be damaged. Also, the top-down method has difficulty with some processes like doping and heterojunction creation. So far, reports of fabricating top-down, Sb-based, 1D nanostructures are based on reactive ion etching (RIE) or focused-ion-beam (FIB) irradiation by chemical and physical means. For example, a porous nanofiber network of GaSb [63], InSb [64, 65] and GaAsSb [66] is fabricated by ion irradiation as a by-product of creating a porous layer. Ion irradiation also can be used to create a randomly distributed, vertical, 1D III-Sb nanostructure [67].

The creation of a periodic, top-down NW array requires a mask to define the shapes, dimensions and position. For example, Kanamori *et al* reported using a patterned e-beam resist as a mask to create a periodic, GaSb nanopillar as subwavelength antireflection gratings by etching the GaSb substrate with a fast atom beam with SF₆ and Cl₂ gases [68]. On the other hand, patterned Au masks were used to create a GaSb nanopillar as small as 20 nm using a BCl₃:Ar plasma etching [69].

Lin *et al* reported a self-mask RIE method to create a GaSb nanopillar below 25 nm [70]. A partially-formed oxide layer was formed on top of the GaSb substrate while being exposed to oxygen plasma which acted as a mask to slow down the etching rate of the protected area. Etching with BCl₃, vertical nanopillars with a diameter under 25 nm and an

aspect ratio up to 24 could be achieved. The authors also compared the etching chemistry between BCl₃/O₂ and Cl₂/O₂ and concluded that using BCl₃/O₂ produced thinner but shorter NWs while Cl₂/O₂ yielded longer but thicker NPs (figure 1(d)). The difference was attributed to the difference between the reaction by-products. The reaction by-products between BCl₃ plasma and the oxide layer were more volatile which led to a smaller oxide mask and faster oxide consumption rate during etching hence resulting in smaller diameters with limited aspect ratio. With Cl₂ plasma, thicker and more tapered NWs were produced. This study highlighted the importance of etching species to the overall morphology of the NWs.

One technique worth noting developed to create highly scaled NWs is called digital-etch which allows the etching of the materials layer-by-layer. It can be worked as a tandem following a bottom-up or top-down approach which creates a relatively larger nanostructure and then further thins down the dimension. Digital-etch includes a series of self-limiting surface oxidation and oxide removal. The technique was used to create sub-10 nm features for a III-As based structure [71, 72]. Though it is such a powerful technique, there is only one report on digital-etch on a III-Sb nanostructure. Usually, the oxide removal agent for III-V digital-etch is a water-based acid that also attacks antimonides, which increases the surface roughness. Lu *et al* developed an alcohol-based etchant to tackle this problem [73]. With the etchant they created, the digital-etch process provided a radial etching rate of InGaSb NW about 1.0 nm/cycle and etched it down to 22 nm. Though the sub-10 nm structure has not been demonstrated so far, the technique is promising and might also apply to other antimonide-based semiconductors.

3. Effect of antimony to NW growth

The development of an antimonide-based epitaxial layer is more challenging than ones for the arsenides and phosphides. One challenge is the limited choice of commercially available substrates that are lattice-matched to the intended grown materials [27]. Also, the properties of Sb, such as low vapor pressure and the surfactant effect, bring up additional difficulties in growing the epitaxial layer [27]. For example, Sb was studied to change the growth dynamic of GeSi film on a Si(001) substrate [74]. With a small concentration of Sb introduced, the lateral growth rate of strained GeSi film was reduced. The growth mode transits from 2D to 3D; that is, the Stranski–Krastanov growth mode is more favorable in the system. The phenomenon can be explained by the decrease in surface diffusion length. The result of those effects is the thicker Ge layer and smaller Ge island [75].

In growing the III-Sb NW counterparts, the process remains challenging. The surfactant effect of Sb changes the NW growth behavior, including the NW morphology and crystal structure, and complicates the process when growing ternary compounds and heterostructures. The low vapor pressure of Sb also makes the growth process difficult to reliably control. In this section, the issues encountered during

the growth of III-Sb NWs are presented as background information and also try to pinpoint the reason why the development of III-Sb NWs lacks behind the III-As and III-P NWs.

3.1. Surfactant effect

III-Sb NWs are known to have a narrower growth window due to the surfactant effect of Sb atoms. As Sb atoms tend to segregate on the surface, the surface energy is modified accordingly. With the shift of surface energy, the growth rate, crystal structure and the preferred preferential growth direction of the shell layer also change. These effects limit further development of the III-Sb NWs.

3.1.1. On axial and radial growth rate. The surfactant effect of Sb is well documented in NW growth. For example, a small concentration of trimethylantimony (TMSb) was found to decrease the growth rate of a Au-catalyzed Si NW in the VLS growth mode [76]. It can be attributed to blocking the incorporation rate of Si atoms due to the surface segregation and hence reducing the growth rate.

The Sb segregation also modifies the contact angle of the catalytic droplet, which is the contact angle between the NW and the catalytic droplet. The change in the contact angle can vary the axial and lateral growth rate of the NWs. The low surface energy of Sb suppresses the contact angle of the catalytic and hence suppresses the axial growth rate.

One typical example is the indium droplet used in self-seeded NW growth. In the self-seeded growth mode of InAsSb NWs, the increase in Sb source vapor pressure reduces the contact angle of the In droplet and hence enhances the lateral growth and suppresses the axial growth rate [77, 78]. The authors of both reports attributed the segregation of Sb to the lowered surface energy of the In droplet and promoted the formation of a nanostructure with high lateral growth rate and a low axial growth rate. The poisoning effect, in which the Sb segregation blocks the incorporation of other atoms to the NW body, might also be attributed to the decrease in the axial growth rate. The reduction in axial growth rate limits the ability to obtain a high-aspect-ratio InAsSb NW with high Sb incorporation.

Except for altering the contact angle of the catalyst particle, the radial growth rate is also boosted in some III-Sb NWs by group III adatoms' adsorption on the NW sidewalls. In GaAsSb NWs, the diffusion length of Ga adatoms was shortened in the presence of Sb, so more of them are absorbed on the (110) side facet instead of diffusing to the catalytic tip, hence enhancing the radial growth and reducing the axial growth [56].

3.1.2. On crystal structure. Controlling the phase purity of a NW is important since it has a huge implication on physical properties and device performance. For III-Sb NWs, the binary compound InSb and GaSb is always in a ZB phase in most of the reports using different techniques like MBE and MOVPE. However, using the same growth techniques, III-V materials like InP, InAs and GaAs are more likely in the WZ

phase or defective WZ phase [79]. Therefore, the incorporation of Sb to these NWs creates a high density of phase impurity or complete phase change [20, 80, 81].

In a ternary Sb-based NW, little incorporation of Sb into InAs and InP, i.e. InAsSb (figures 2(a)–(e)) and InPSb (figure 2(f)), induces high density of stacking fault and twinning [20, 81]. The defect density can be adjusted by the Sb concentration. Taking Au-catalyzed InAs/InAs_{1-x}Sb_x as an example system, Xu *et al* showed a clear transition from pure WZ InAs NW to a WZ and ZB mixture with a high density of twinning ($x = 0.03$ to 0.08) to pure ZB InAs_{1-x}Sb_x (when $x = 0.12$) (figures 2(a)–(e)) [81]. A similar effect was also observed on self-catalyzed InAs_{1-x}Sb_x NWs which showed it was not an Au-catalyst induced phase change [47, 82].

In recent research, the WZ-to-ZB transition is related to the change of contact angle under higher Sb precursor flux. The diameter of the catalyst particle is increased under a higher Sb precursor flux which in turn decreases the contact angle in both Au-catalytic or self-catalytic growth [27, 56, 82]. Hence, the surface energy of the liquid (catalyst)-solid (NW) and liquid-vapor (source flux) are modified [56, 82]. Under high Sb flux, the surface energy modification favors ZB phase formation which leads to perfect ZB NWs when a certain threshold is reached.

3.1.3. On preferential growth direction. To integrate the NWs into optoelectronic devices, creating core-shell heterostructures is an important step. The fabrication of III-As, III-P and III-N core-shell structures is better-developed than their III-Sb counterparts. For III-Sb NWs, the surfactant effect of the Sb changes the facet geometry and polarity of the core-shell NW structures obtained [83]. Yuan *et al* show the InP shell layer preferably grows along {112}B facets of hexagonal GaAsSb NW instead of {112}A facets which results in a triangular shape core-shell NW structure. For a typical GaAs core, the InP grows along the $\langle 110 \rangle$ directions which have the lowest surface energy. For GaAsSb, the presence of Sb modified the surface energy of different facets, i.e. the {112}A facets become the plane with the lowest surface energy and have a faster growth rate while the growth rate in $\langle 110 \rangle$ directions is reduced. The {112}B facets have the highest surface energy, so the InP growth is suppressed. A similar phenomenon was also observed during the growth of a GaAs/GaAsSb quantum well NW which limits the shell thickness when it is necessary to create a core-multishell structure [84].

3.2. On surface morphology

The V/III ratio during the growth of III-V NWs is the key to adjusting the axial and radial growth rate. Therefore, the surface morphology of III-Sb NW is heavily dependent on the V/III ratio. In the study of growing GaAs/GaSb heterostructure NWs in MOVPE [27, 85], the surface morphology and radial growth rate of the GaSb segment change with the supply ratio of Ga and Sb precursors. With the V/III ratio changed, the GaSb can be tuned between straight, thin NW,

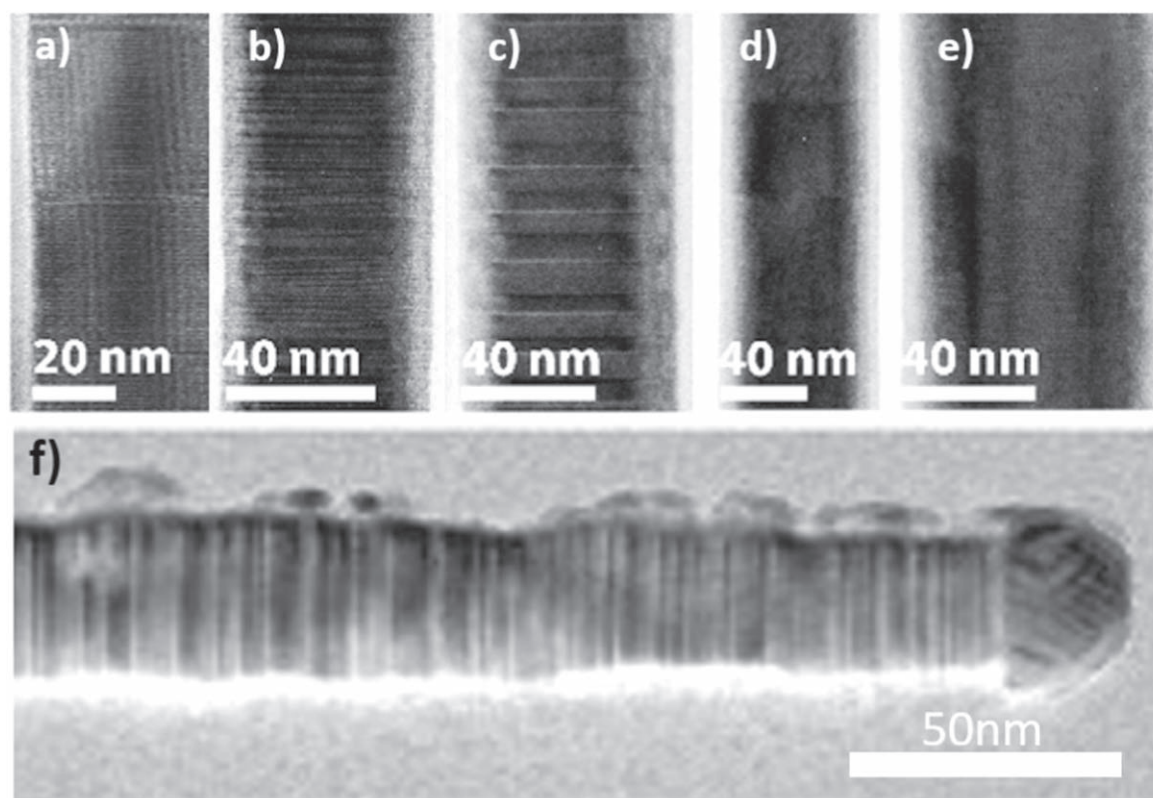


Figure 2. (a)–(e) Sb-induced phase transition of $\text{InAs}_{1-x}\text{Sb}_x$ NWs where $x =$ (a) below x-ray energy dispersive spectroscopy (XEDS) detection limit, (b) 0.03, (c) 0.05, (d) 0.08 and (e) 0.12 [81] (reproduced from [81]. © IOP Publishing Ltd. All rights reserved). (f) High-resolution transmission electron microscopy (HRTEM) image of an $\text{InP}_{1-x}\text{Sb}_x$ NW. Large number of plane defects are observed [20] (reprinted from [20], Copyright 2011, with permission from Elsevier).

thicker NW, kinked NW or the irregular GaSb shell grown around the GaAs stem [27].

In another study for InSb NWs, the authors discovered that the radial growth rate of InSb NW was increased with the increase of the V/III ratio. Therefore, under a high V/III ratio, an InSb nanocube is grown instead of the NW because of rebalancing the axial and radial growth rate [86]. The authors further studied the morphology evolution by adjusting the interdistance of the NW growth site. A similar effect was observed due to the change in the local V/III ratio.

3.3. Low vapor pressure of Sb

To grow III–V material, a controllable supply of group V and group III elements is necessary. The ratio between the two groups of elements is called the V/III ratio. In growing III–As and -P bulk materials using techniques like MBE and MOCVD, the V/III ratio is always high to maintain a sufficient supply of group V elements. Due to the high vapor pressure of As and P, the condensation of the elements is limited even under a high V/III ratio environment. It is not the same case for Sb due to its low vapor pressure. Elemental Sb tends to stick on the growth substrate and form Sb crystallites [87].

The low vapor pressure of Sb compared to As and P poses some challenges when growing an axial heterostructure with an As-contained or P-contained junction. For example, regarding the growth of an InAs/InSb NW, even though the

As supply is closed during the growth of the InSb segment, the InSb still contains a few percents of As. It suggests that the incorporation of As come from the As precursor residual in the background due to the high V/III ratio environment during the stem growth or the decomposition of the As-contained stem [88, 89].

Another problem arises from the decomposition of the III–As stem in an As-limited regime during the growth of a III–Sb segment with high Sb flux. It has been observed in several reports. For example, when growing an InAs/InAsSb axial junction in MOVPE, the NW density growing under a very low AsH_3 supply is lower which indicated that the NW was broken during the growth [90]. In another report when growing GaAs/GaAsSb NW under an As-limited growth environment, the GaAs stem became thinner; this was attributed to the decomposition of the GaAs segment [50]. During the growth of InSb NWs on an InP/InAs stem, the decomposition of the InAs segment limited the final length of the InSb NWs [91].

3.4. Memory effect

Another problem that arises from growing III–Sb-based materials is the memory effect. It happens after growing a Sb-rich structure and following it up by growing a non-Sb structure in the same chamber. The cause of memory effect is discussed elsewhere [27]. In brief, the low vapor pressure of the Sb requires a longer purging time and sufficient heating to

desorb the remaining Sb inside the growth chamber. The residue changes the growth behavior of the epitaxial layer. For example, in bulk form, a Sb-containing heterostructure is known to cause a graded interface for a heterostructure in bulk form due to the existence of a Sb surfactant layer [92].

The memory effect still exists when growing antimonide NWs. For NWs, the residual Sb might come from a residual TMSb precursor, decomposition by-products of the precursor [93] or the Sb traces remaining in the catalyst [94]. A certain amount of Sb dissolves in the metal catalyst tip, and when the Sb incorporates into the catalyst particle, the growth behavior of the non-Sb junction will be changed. In a report, the researchers claimed the Sb residual from the background made the growth of InAs NW right after the growth of the InSb segment challenging [93]. To eliminate this effect, the authors grew all the InAs NW stems under pre-designed conditions one by one and stored them in the store chamber. After that, the InAs NW samples were reintroduced to the growth chamber to grow the InSb NWs. In another study [94], the authors suggested WZ-to-ZB transition of perfect GaAsSb to a stacking fault containing GaAs segment is due to the remaining Sb in the catalytic particle.

The memory effect needs to be taken care of in order to ensure the smooth fabrication process of Sb-containing junctions and Sb-less junctions. Careful design of the growth condition or growth chamber cleaning is necessary to prevent such an effect [27].

4. Recent progress in III-Sb NWs development

In this part, some recent progress of III-Sb NWs is presented. This includes phase engineering, NW morphology control and composition engineering. The NW network formation and interface engineering of InSb NWs are also reviewed which only focused on MZM related research but might also benefit other applications.

4.1. Phase engineering

In this section, we will review the development of the phase engineering of III-Sb NWs regarding WZ phase formation which has not been achieved before. Also, the creation of twinning superlattices is also reviewed. The understanding of how to create these structures will benefit the integration of electronic and optoelectronic applications.

4.1.1. WZ formation. The crystal structures of III-V materials are either ZB or WZ in most of the cases. ZB is a cubic lattice system in which atoms occupy ABCABC sites while WZ is a hexagonal lattice system in which atoms occupy ABAB sites. The optical and electronic properties of these two crystal structures are different [95–99]. For example, the bandgap of WZ phase III-V materials is always higher than that of their ZB counterparts [100]. Another example: AlSb in the WZ phase is predicted to be a

direct bandgap material while its ZB counterpart is an indirect bandgap [98].

For various applications, the difference in crystal phases means different device performance. In a detailed study conducted using transmission electron microscopy (TEM) which is also capable of doing electrical measurement, ZB InAs NW transistors have a lower on-off ratio but higher field-effect mobility, conductivities, and electron concentration when $V_{BG} = 0$ V [99]. On the other hand, Ullah *et al* reported the performance difference of a WZ and ZB InAs NW transistor under different atmospheres [101]. Also, WZ InAsSb NWs are predicted to have better spin-orbit coupling than the ZB structure [102]. Therefore, the capability of fabricating a WZ III-Sb NW is important in terms of application aspects.

Depending on growth conditions, the crystal structure of III-V NWs can be switched between a ZB and WZ structure. For III-As and III-P NWs, the WZ NWs are easier to be obtained. III-As and III-P WZ NWs can be obtained by using a higher growth temperature [79], lower V/III ratio [103] or NW diameter restriction method [104, 105]. However, III-Sb NWs are more favorably grown in the ZB phase. In earlier reports, the WZ phase was achievable but not in a controllable manner [46, 106, 107]. One possible reason for this is that III-Sb has the lowest ionicity among all the III-V materials. Generally speaking, materials with higher ionicity are more likely to form a WZ structure like III-nitride while a ZB structure is more favorably formed in materials with lower ionicity like III-Sb [46].

As mentioned earlier, one reported strategy to grow a III-As or III-P WZ NW is to restrict the NW diameter. However, the same strategy so far does not apply to III-Sb NWs. In the previous report, InSb NWs with diameters down to sub-10 nm were fabricated using CVD but the NW is still in the ZB phase [108]. On the other hand, the WZ phase was found in very thick NWs (200–300 nm) with careful control of the growth conditions [46]. In the research of Mandl *et al* using the self-seeded approach, an InSb NW with a WZ phase was obtained. By observing the NW structure with a different growth time, they concluded that the amount of Sb incorporation in the In catalytic tip controlled the structure of the NW. High supersaturation in the In-Sb particle favors the WZ structure growth [46].

Ghalamestani *et al* demonstrated the growth of WZ InSb NWs by decreasing the V/III ratio by two approaches [109]. In their report, they firstly suppressed the molar fraction of the group V source (in this case, TMSb) in the chamber which is a generic approach to grow WZ phase III-As and III-P NWs. During the growth of InSb NWs, the supply of the TMSb was gradually decreased, and the obtained InSb NWs showed a phase transition from ZB to 4H to WZ. After that, they also used a pulsing growth approach to limit the Sb supply inside the reactor. In that approach, the indium source supply trimethylindium (TMIn) was kept constant while the antimony source (TMSb) was supplied for a certain period for a certain number of cycles. With careful adjustment of the growth parameters like the pulse off time and Au particle size, a WZ segment was also obtained. However, during further attempts to grow a

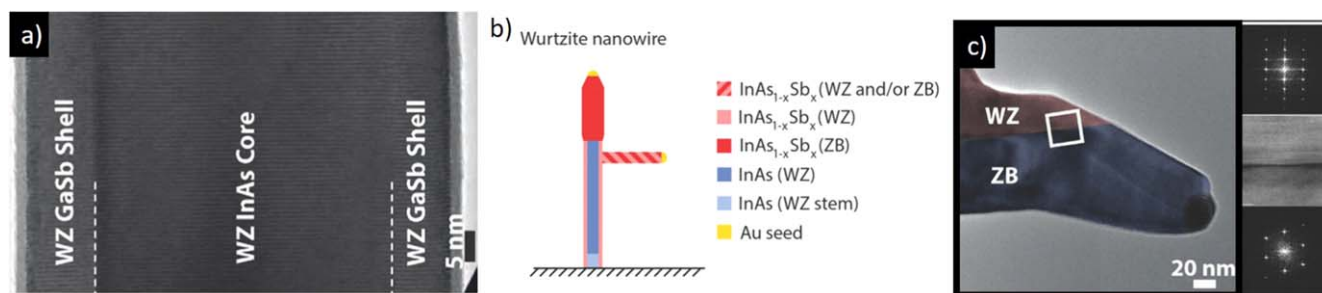


Figure 3. (a) HRTEM image of a WZ GaSb shell grown on a WZ InAs core [111] (John Wiley & Sons. © 2018 WILEY-VCH Verlag GmbH & Co. KGaA, Weinheim). (b) Schematic of a WZ InAs_{1-x}Sb_x branch grown on an InAs trunk [90]. (c) False colored HRTEM image of InAs_{1-x}Sb_x grown on an InAs WZ NW where the WZ and ZB phases coexisted. Insets are diffraction patterns of the WZ (top) and ZB (bottom) phase regions. The inset in the middle is the HRTEM image of the phase interphase marked in the white box [90] (John Wiley & Sons. © 2018 WILEY-VCH Verlag GmbH & Co. KGaA, Weinheim).

ZB-WZ-ZB structure, the WZ segment disappeared/transformed during the prolonged ZB segment growth (3:45 min), which suggested careful process management was needed to preserve the WZ segment. The authors suggested that a Sb-limited environment, high group III content in the catalytic particle, and certain wetting angles were necessary to grow a WZ phase InSb segment. They also tried to grow GaSb WZ NWs using a similar approach. However, no WZ phase was observed except for a few twin planes. The authors suggested a similar effect that happened on InSb NW might also possibly occur with GaSb NWs. However, the conditions were much more limited, and the attempt did not succeed.

Another approach to grow III-Sb in the WZ phase is to use a WZ phase III-V NW as an underlying template [110]. As the III-Sb shell layer grows along the already existing facet epitaxially, the shell layer is also in the WZ phase. This method has been demonstrated in several WZ III-V core/III-Sb shell systems like InAs/InAsSb NW [110], and InAs/GaSb (figure 3(a)) [111], GaAs/GaAsSb [112] and InAs/AlSb NWs [14]. In the report of Kindlund *et al* [14], the growth of a AlSb WZ shell is more favorable than the ZB counterpart at a decreasing temperature as a consequence of the kinetic limitation of the AlSb shell growth.

Apart from being used as a growing template of the III-Sb shell layer, III-V WZ NW can also be used as a nucleation site of new III-Sb WZ NW. There are two reports about growing WZ phase InAsSb NWs on an InAs WZ NW template. In a report by Dahl *et al* [90], the WZ segment of InAsSb NW was grown on an InAs WZ trunk using a secondary Au seed particle by MOVPE (figure 3(b)). The WZ InAs NWs' trunk was first grown using a Au seed particle. Secondary Au seed particles were then deposited on the WZ NW trunk and the growth of a branch structure started. The authors discovered that both WZ and ZB structures existed (figure 3(c)) in the InAsSb branch and that it was nucleated from the stacking fault which might suggest the secondary Au seeds on the sidewall migrated to the stacking fault and then the growth started. One interesting observation was that during the growth of the InAsSb branch, the Au seed particle was pushed to the ZB side while the WZ structure growth was eliminated eventually (figure 3(b)). It is because the growth of the ZB structure is more favorable than the WZ structure.

In another report [102], Sestoft *et al* used the (1–100) side facet of an [0001] InAs WZ NW to grow InAs WZ NW. The Sb precursor was then introduced to the chamber to nucleate the growth of InAsSb NW. As the growth direction of the InAsSb NW was locked by the top facet of the InAs WZ NW, the InAsSb segment remained in the WZ phase.

4.1.2. Twinning superlattice. The twinning superlattice is predicted to be a desirable structure for thermoelectric applications because it increases the difficulty of phonon transfer in the structure [113, 114]. It may also be beneficial for some electronic and optoelectronic applications. For III-As and III-P NWs, twinning superlattice structures have been realized by Zn-doping [115, 116] or by adjusting the growth parameters [95, 117] to change the surface energy. The growth of the InSb NW twinning superlattice has been realized recently. Using a solution route, Qian and Yang fabricated an InSb twinning superlattice NW under a relatively low temperature [45]. The superlattice formation was found to be related to the reduction rate fluctuation of an In and Sb source periodically. The twinning superlattice NWs showed high electron carrier concentration on the surface and ultrafast responses in photoconductive measurement despite the growth under such a low temperature.

In another report, Yuan *et al* fabricated twinning superlattice InSb and InP NWs using Au-catalyzed MOVPE [118]. By careful adjustment of the growth parameters like the V/III ratio and total precursor flow, the shape and the contact angle of the Au catalyst were manipulated which triggered the growth of a twinning superlattice. The manipulation of the contact angle changes the surface energy which is similar to the Zn-doping route. This method is expected to apply not only to InSb NW but also to III-Sb and In-V NWs due to their low surface energy, as demonstrated with the InP twinning superlattice in the same report [118].

4.2. Morphology control

4.2.1. Diameter suppression. For some applications like electronic devices and Marjona detection, a NW with several tens of nanometer in diameter is essential. However, the diameters of III-Sb NW are always larger than those of the

III-P and III-As counterparts. In earlier reports, binary III-Sb NW with a very small diameter is attainable (5 nm for InSb NWs [108] and 25 nm for GaSb NWs [45]). However, the diameter distribution in these reports is rather large which is not desirable for large-scale device integration. Trimming down the NW size becomes an important task to be tackled.

There are several reasons behind the diameter enlargement in III-Sb NWs. First of all, the catalyst particle of III-Sb NWs has a larger size than the III-P and III-As counterparts which leads to a larger corresponding NW diameter. The catalyst particle tends to absorb a higher amount of the group III element during the growth of III-Sb NWs [28, 85]. Also, Sb incorporates in the catalytic particle and leads to thicker NW diameters [46, 106]. Furthermore, it is commonly observed that increasing the V/III ratio (increasing the Sb supply for III-Sb NW while keeping the group III precursor unchanged) would also increase the radial growth of III-Sb NW, as described in the earlier section. Another factor, unexpectedly, is that the length of stem size also affects the NW morphology. As reported by Pea *et al.*, a longer InAs stem increases the overgrowth of InAsSb NW [119]. These effects limit the minimum attainable NW size. Therefore, it is important to discover how to fabricate thin NWs with a narrow diameter distribution. Here some reports are outlined that discuss the suppression of the radial growth rate.

To grow thin III-Sb NW, it is important to carefully adjust the growth conditions like growth temperature and Sb precursor supply. Ek *et al.* demonstrated that by adjusting the growth temperature and the partial pressure of TMSb (Sb precursor), the nucleation yield, GaSb NW diameter and growth rate can also be adjusted in a MOVPE [120]. They found that with higher growth temperature or TMSb partial pressure, the critical GaSb NW size grown on an InAs stem could be lower due to lower supersaturation in a Au particle. In their report, they showed that by minimizing the InAs stem size (down to 21 nm) and increasing the TMSb partial pressure, thin GaSb NW (32 nm) could be grown with high yield.

Yang *et al.* used a sulfur surfactant to stabilize the sidewall of GaSb NWs during the growth process in a tube furnace [121]. They compared the GaSb NWs with and without the use of a sulfur surfactant. Without sulfur, the GaSb NWs had a much larger diameter (219 nm in average) and the NW was tapered. With the use of a sulfur surfactant, the diameters were drastically smaller (24 nm in average) and had a smooth surface without tapering. The authors attributed that the S atoms bonded with the unsaturated Sb atoms on the surface and formed stable S-Sb bonds. As the sidewalls of the GaSb NWs were stabilized, the undesired radial growth was suppressed. In a further study [44], they replaced the Au catalyst with Pd (figure 4(a)). By employing the Pd catalyst, the growth mode of the GaSb NW switches from a VLS mode to VSS mode. The cylindrical PdGa alloy catalyst particle further narrowed down the diameter distribution and the NW orientation (figures 4(b) and (c)).

Growing III-Sb NWs in a predefined template is another strategy to suppress the radial growth. As described in the previous section, TASE is a method to confine the NW

dimension because the NW is grown inside a SiO₂ channel [61]. The dimension of the channel restricts the radial growth of the III-Sb NW. Therefore, by controlling the dimension of the SiO₂ channel, the NW dimension can be controlled. In a previous report, InAs NWs with a thickness of 23 nm were fabricated [61]. Recently, it was demonstrated that the same technique could be applied to grow GaSb NW. With this method, the obtained GaSb NWs' structure with the width down to 20 nm could be fabricated (figure 1(c)) [62].

4.2.2. Morphology control by adjusting the pitch distance. As described in an earlier section, the SAG mode is a method commonly used to fabricate a NWs array on top of the crystalline substrate without foreign catalyst incorporation. It also provides some room to adjust the morphology and optical properties of III-Sb NWs.

In the SAG growth mode, as the interdistance of the pitches can be adjusted precisely, some properties of the III-V NWs can be tuned accordingly [122, 123]. In III-Sb NWs, the pitch distance-dependent effect is more pronounced. Plissard *et al.* controlled the shape of an InSb nanostructure from NW to nanocube by adjusting the interdistance of the NW stem [86]. The authors attributed the morphology evolution to the 'local' V/III ratio change. As the TMSb has a shorter diffusion length, the NW array with the shorter interdistance will suffer from a lower 'local' V/III ratio due to greater competition [124]. Therefore, the growth rates (both radial and axial) are decreased and hence the shape of the InSb nanostructure can be tuned accordingly. In recent years, there have been several reports about adjusting the pitch distance to modulate the optical properties of GaAsSb NWs. Apart from the change in growth rate, the composition of GaAsSb NWs is also dependent on the pitch interdistance. As mentioned earlier, the existence of Sb changes the absorption efficiency of the group V element and hence the composition's As/Sb ratio [56, 125]; the optical properties of the GaAsSb NW array is also changed by the NW interdistance. In micro-photoluminescence (u-PL) measurements, the GaAsSb NW array with smaller pitch length shows a redshift compared to a larger pitch length [125]. A similar redshift effect was also observed when the location of the GaAsSb NW shifts from the corner to the center of the array, which offers important guidance regarding the design of the NW array.

4.3. Composition engineering of ternary III-Sb NW

The physical properties of ternary NW are dependent on the composition. The composition tuning of the ternary III-Sb NWs provides flexibility to properties engineering which is important for optical and electrical applications. Table 2 shows some examples of the composition range of InAs_{1-x}Sb_x and GaAs_{1-x}Sb_x NWs attained by different reports.

For InAs_{1-x}Sb_x NWs, full-composition tunability has already been demonstrated in an earlier report. Ercolani *et al.* grew InAs/InAs_{1-x}Sb_x axial NW using gold nanoparticles as a catalyst in a chemical beam epitaxy (CBE) system [126]. By tuning the flux fraction of tert-dimethylaminoantimony

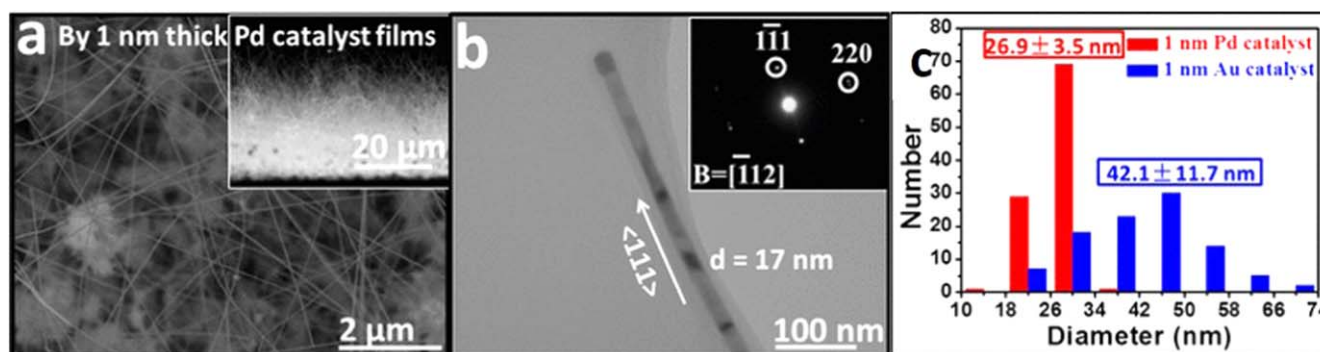


Figure 4. (a) SEM image of Pd-grown GaSb NWs. Inset show the cross-section SEM image of the same sample. (b) TEM image of a Pd-grown GaSb NW. Inset shows the corresponding diffraction pattern. (c) Diameter statistics of Pd- and Au-grown GaSb NWs [44] (adapted with permission from [44]. Copyright 2017 American Chemical Society).

(TDMASb) and tertiarybutylarsine (TBAs), the x value could be tuned from less than 0.1 up to 0.7 (InAs/InSb NWs were also reported by the same group [89]) (figures 5(a)–(c)). Other than this report, several other reports also realize InAsSb with a wide x range using gold as a catalyst with an InAs stem in MOVPE [127]. With stemless InAs_{1-x}Sb_x NWs directly grown on an InAs(111)B epi-ready substrate using MOVPE, x can be as high as 0.75 [128]. Further decreases in the molar fraction of AsH₃ to a certain level yield very short NWs or no NWs can be nucleated at all.

Although InAs_{1-x}Sb_x NWs achieve a wide x range using Au as a catalyst, full-composition range growth is not observed by self-seeded growth or the SAG growth mode yet. Growing InAs_{1-x}Sb_x NWs with the self-seeded method (which is using an In droplet as a catalyst) with a high x value remains challenging at the moment. As discussed earlier, the surfactant effect of Sb reduced the axial growth rate and promoted the lateral growth rate of the NWs when using an indium droplet as a catalyst. Using MOVPE, a flat InAs_{1-x}Sb_x pillar with x as high as 0.43 was grown on Si (111) substrates [77]. Other reports using the self-seeded method seldom went over 0.2 [48, 78, 129].

Using the SAG growth mode, 14.5 nm SiO₂ was deposited on GaAs(111)B substrates by spin-coating and annealing hydrogen silsesquioxane (HSQ) as a mask to nucleate the growth of InAs_{1-x}Sb_x. An x value as high as 0.35 was achieved [16, 130].

GaAs_{1-x}Sb_x NWs have been grown using various approaches. For example, using a gold catalyst, GaAs_{1-x}Sb_x with Sb% as high as 60% was grown by MOCVD and MOVPE [131]. The self-catalyzed method was also used and the Sb% is below 50% [94, 132].

In a recent report, a near full-composition-range ($0 \leq x \leq 0.93$) of GaAs_{1-x}Sb_x was achieved on Si(111) substrates using MBE (figures 5(d)–(g)) [50]. The authors first studied growing GaAs_{1-x}Sb_x directly on top of Si(111) substrates by tuning the flux of one group V supply (As or Sb) while keeping the other constant to increase the Sb content. By increasing the Sb flux, As-rich GaAs_{1-x}Sb_x ($0 \leq x \leq 0.35$) was obtained while GaAs_{1-x}Sb_x with $x \leq 0.6$ was achieved by decreasing the As flux (figure 5(d)). For the growth of the GaAs_{1-x}Sb_x with the GaAs stem, however, only short and

tapered NWs with x as high as 0.5 were grown by lowering the As flux to 9.75×10^{-7} Torr. Further lowering the As flux yielded no NWs on the GaAs stem. To reach $x > 0.6$, the authors shut down the As flux. Instead, the As source was supplied by the background. By tuning the As background, $0.54 \leq x \leq 0.93$ was achieved (figure 5(e)).

Ga_{1-x}In_xSb NW is another promising system for electrical application. Ghalamestani *et al* grew Ga_{1-x}In_xSb NWs on a GaAs/GaSb stem, which showed that full-composition range tunability (x from 0.03 to 1) was achievable [19]. In another report from the same group, on an InAs/InSb stem, the x is from 0.3 to 1 [18].

In conclusion, ternary III-Sb NWs with a wide-range x value can be obtained. However, reaching the wide composition range requires suitable design and a growth method which includes the choice of NW stem used, shutting down the supply of one group V element and fine-tuning the growth parameters. The non-gold foreign catalyst for ternary III-Sb NWs has not yet been explored. Also, achieving a high x for self-catalyzed InAs_{1-x}Sb_x NW still needs to be developed.

4.4. Toward quantum computation

The manipulation of MZMs might be the key to achieving topological quantum computation. The high g -factor and low effective mass of InSb-based (and also InAs) NW make it an ideal platform to search for MZMs research.

The first observed signature of MZMs was reported in 2012 on an InSb NW device [91]. After that, researchers have tried to look for more MZM signatures or to gain better control of them. The strong spin-orbit coupling and large g -factor of InAs and InSb make them ideal materials to realize topological superconductivity and MZMs, especially in their NW form. However, to investigate MZMs, a good quality NW network and semiconductor/superconductor interface are necessary to ensure the nearly ballistic transport. Also, unwanted Majoranas might be induced by defects in the wires and interface. This part focuses on the work done towards creating an InSb NW network and the semiconductor/superconductor interface engineering of an InSb NW device. These are important developments toward spin-based quantum computation. A more in-depth review of the recent status of MZMs is referred to [4].

Table 2. Composition range of $\text{InAs}_{1-x}\text{Sb}_x$ and $\text{GaAs}_{1-x}\text{Sb}_x$ NWs attained in different reports.

Material	Method	Growing System	Stem	Substrate	Composition Range (x)	References	Remarks
$\text{InAs}_{1-x}\text{Sb}_x$	Au-catalyzed	CBE	InAs	InAs(111)B	Less than 0.1 up to 0.7	[126]	InAs/InSb NWs were reported in [89]
	Au-catalyzed	MOVPE	InAs	InAs(111)B	$0.08 \leq x \leq 0.77$	[127]	
	Au-catalyzed	MOVPE	No stem	InAs(111)B	$0.08 \leq x \leq 0.77$	[128]	Further increase in x results in no NW
	Self-seeded	MOVPE	No stem	Si (111)	$0 \leq x \leq 0.43$	[77]	Flat pillar when $x=0.43$
	Self-seeded	MBE	No stem	Si (111)	Up to 0.10	[78]	Further increase in 2D film
	Self-seeded	MOCVD	No stem	Si (111)	~ 0.33	[129]	VLS growth mode
$\text{GaAs}_{1-x}\text{Sb}_x$	Self-catalyzed	MBE	No stem	GaAs(111)B	$0 \leq x \leq 0.36$	[16, 130]	
	Au-catalyzed	MOVPE	GaAs	GaAs(111)B	$0.09 \leq x \leq 0.6$	[131]	
	Self-catalyzed	MBE	No stem	Si (111)	$0 \leq x \leq 0.44$	[132]	
	Self-catalyzed	MBE	GaAs	Si (111)	Up to 0.34	[94]	
	Self-catalyzed	MBE	No stem	Si (111)	$0 \leq x \leq 0.6$	[50]	Further reduced As flux results in film
	Self-catalyzed	MBE	GaAs	Si (111)	$0 \leq x \leq 0.5$	[50]	No NW grown when $x > 0.55$
	Self-catalyzed	MBE	GaAs	Si (111)	$0.54 \leq x \leq 0.93$	[50]	As from the background

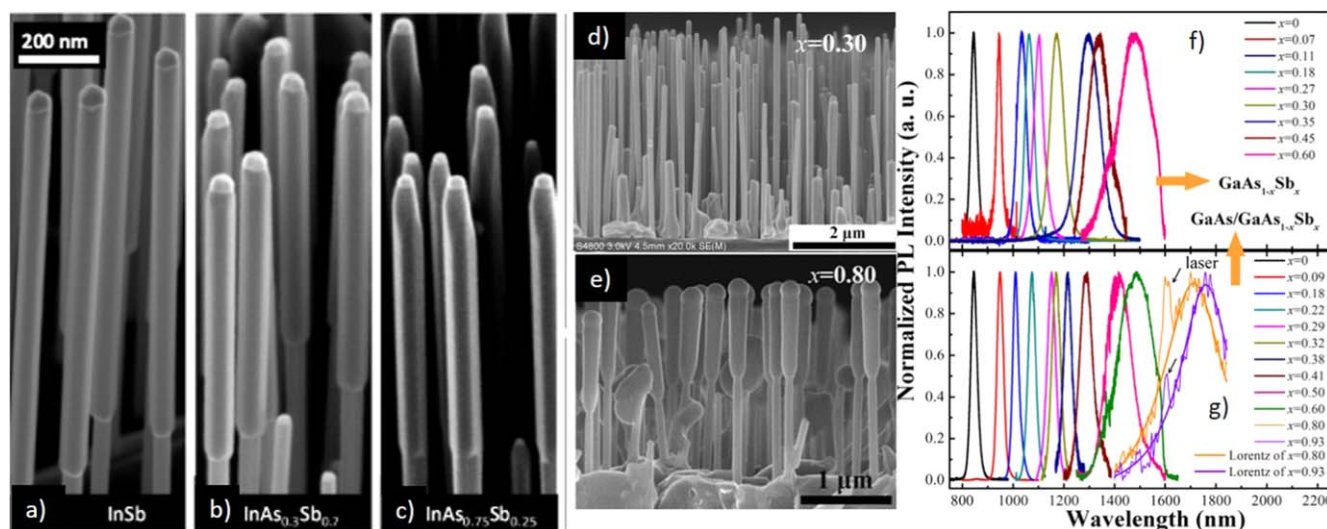


Figure 5. (a)–(c) SEM images of InSb, InAs_{0.3}Sb_{0.7} and InAs_{0.75}Sb_{0.25} NWs grown on InAs NW stems grown by CBE [126] (reproduced from [126]). © IOP Publishing Ltd. All rights reserved). (d) Side-view SEM image of self-catalyzed GaAs_{1-x}Sb_x NW grown on Si(111) $x = 0.30$. (e) Side-view SEM image of self-catalyzed GaAs_{1-x}Sb_x NWs grown on GaAs NW stems with $x = 0.8$. (f) and (g) The bandgap of GaAs_{1-x}Sb_x NW with a different x value measured by photoluminescence (PL) at 77 K [50] (adapted with permission from [50]. Copyright 2017 American Chemical Society).

4.4.1. Creating a NW network. One straightforward way to create a NW network is by a top-down approach. However, good quality epitaxial film is hard to grow. Also, an adequate etching process still needs to be developed [4].

Aside from lithography-based top-down techniques, creating complex NW networks by VLS-based bottom-up methods also draws huge attention. Various growth schemes are developed to create monocrystalline InAs and InSb NW networks.

One way to create a NW network is by merging multiple NWs during NW growth. To interconnect the bottom-up NWs, precise control of the NWs' position and their merging angle is of paramount importance. The latter part requires the capability of controlling the growth orientation which is usually done by creating inclined NWs. Based on the experience of the NWs' growth, various growth schemes are developed to create inclined InAs and InSb NWs which include manipulating the growth substrate's orientation [133]; for example, inclined InAs NWs can be grown on an (001) InAs substrate. As a large amount of NWs are grown together, there is a certain possibility that InAs NWs merge and form a T-junction and K-junction [133]. The inclined NW can also be grown on a sloped facet [134, 135] or by using a kinked NW stem as the growth site [136]. For an InSb NW, an InP NW stem is needed for nucleation. After creating inclined NWs, the well-positioned catalytic site is essential to increase the yield of NWs merging to form the NW network. It can be done by lithography-based positioning. Another concern of these NW networks is the crystallinity. Non-optimized design of the NW phase and the growth orientation result in phase transformation or defects formation which is undesirable [134, 136].

Plissard *et al* fabricated InSb nanocrosses using a vertical Au-catalyzed InP/InAs stem as a base [91]. After growing the

InP/InAs stem, the NWs were then annealed so that the Au-tip slipped to one of the {112} side facets and the InSb NWs were grown on those facets horizontally. T or X shape junctions were formed when the InSb NWs met and merged. A single crystalline structure could be formed when the crossing angle of two InSb NWs was 70.5° (a twin junction might also form depending on the polarity orientation of the wires). The yield of single crystalline structure in this report was low. To further improve the yield, the same group patterned the catalyst position by electron beam lithography on the InP (001) substrate [137]. As the InP stems preferred to grow in the two <111> B direction, the chance for two NWs merging at 109.5° increases to 25% (figure 6(a)). In this report, the authors also found that a certain offset of the catalyst position was needed to prevent the formation of a bridge junction when two catalytic-tips merged (figure 6(b)). The crystal quality of the junction is high (figures 6(c)–(e)). An even more complex 'hashtag' InSb NW structure was reported in 2017, using RIE and followed by wet-etching to expose the InP (111)B facets [138]. The InP stem and the InSb NW grew along the (111)B facets on predefined catalyst sites and were forced to meet at the destined position and merged to form a complex nanostructure. More complex structures can be formed by controlling the trenches' dimension and spacing. These complex network structures show Aharonov–Bohm and weak-antilocalization effects under quantum transport measurement which proves that these networks are phase-coherent and which shows strong spin–orbit coupling [138].

4.4.2. Semiconductor-superconductor interface engineering.

In previous reports [91, 139], the signature of Majorana particles was observed in semiconductor-superconductor NW devices. To realize the MZMs, the fabrication of a

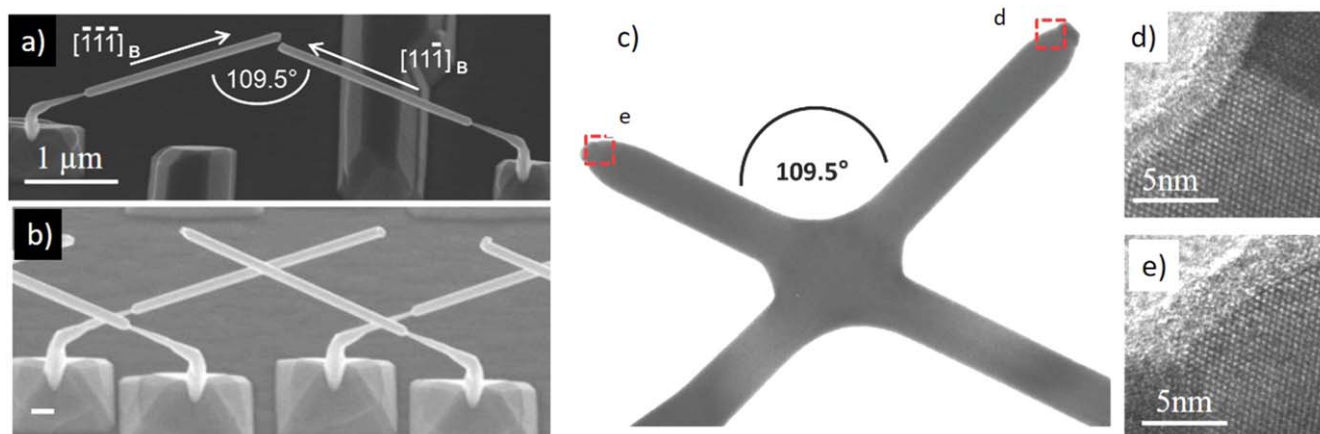


Figure 6. (a) Two InSb NWs grown in $\langle 111 \rangle_B$ directions and which are 109.5° with respect to each other. (b) Tilted angle view of an InSb NW cross junction. The scale bar represents 200 nm. (c) TEM image of an InSb NW junction. (d)–(e) HRTEM images of a selective region indicated in (c) [137] (John Wiley & Sons. © 2014 WILEY-VCH Verlag GmbH & Co. KGaA, Weinheim).

high-quality semiconductor and superconductor (usually Al or NbTiN) interface needs to be developed. In this session, research into III-Sb NW-based devices is highlighted from the device fabrication perspective to review the progress of MZMs studied.

Earlier reports used sputtering or evaporation to create electrodes without any interface engineering [91, 140, 141]. However, these devices show a soft superconducting gap which degrades the topological protection. One of the possible sources of the existing soft gap is the interface inhomogeneity like the formation of native oxide on the NW surface [142]. Therefore, to reduce the subgap states, the interface of the semiconductor and superconductor electrode must be of high quality. To improve the interface quality, diluted ammonium sulfide solution was used to passivate the InSb NW surface in two reports [143, 144]. Ammonium sulfide solution is commonly used to remove the native oxide as well as passivate the surface dangling bond of a III–V semiconductor [145]. However, as the passivation is an *ex situ* process, the passivation effect is not satisfied.

Further improvement is achieved by cleaning the sulfur-cleaned InSb NW surface with *in situ* low-power argon cleaning and then depositing a thin wetting layer (5 nm of NbTi) before the deposition of the NbTiN electrode. The device shows lower contact resistance, hard superconducting properties and a supercurrent under ~ 0.5 T of magnetic fields [144]. Using a similar treatment sequence [146], the InSb device shows clear ballistic transport properties. In another report [147], Gill *et al* deposited an Al shell epitaxially on a selective area of the InSb NW after S-cleaning and low-power argon cleaning. The obtained device showed high interface quality and exhibited a hard superconducting gap and near no-loss transmission of the supercurrent in a single-mode regime. A high-quality interface could also be achieved by *in situ* atomic hydrogen treatment which has been demonstrated to be an alternative way to remove the native oxide under ultrahigh vacuum under a relatively low temperature (300 °C) [148].

Another method is to produce a high-quality interface to grow an Al epitaxial layer around the NW right after the NW has grown without breaking the vacuum, as has been performed on InAs NWs [102]. In a recent report, the growth of an Al shell on both ZB and WZ InAsSb NWs is studied. With an increasing amount of Sb incorporation in InAs NW, the relative orientation of the Al shell changes. The structure shows a hard gap induced superconductivity which is consistent with topological phase transitions.

5. Applications of III-Sb NWs

So far, the properties, growth and some recent progress of III-Sb NWs have been discussed. Due to a deepened understanding of how to manipulate growth and properties engineering, combined with the excellent electrical and optical properties of III-Sb NWs, various applications have been realized in recent years.

For example, InSb NWs were used to fabricate a NO₂ sensor [149] and thermoelectric [150, 151]. In this part, the recent progress of electronic and optoelectronic applications of III-Sb NWs will be discussed.

5.1. Electronics applications

The high electron mobility of InSb and the high hole mobility of GaSb make them and their alloys intriguing candidates for high-speed and low-power electronics. Field-effect transistors (FETs) are nowadays essential components in everyday life. A major application of FETs is data processing. The development of A.I., big data analytics and blockchain technology create huge demands of computation power which make the development of high-frequency and low-power consumption electronics necessary.

Developing a NWFET provides several advantages. For example, the implementation of a gate-all-around (GAA) structure provides good electrostatic control. Also, as the fabrication technique becomes more mature, materials with a wider range of options (like diameter and composition) can be

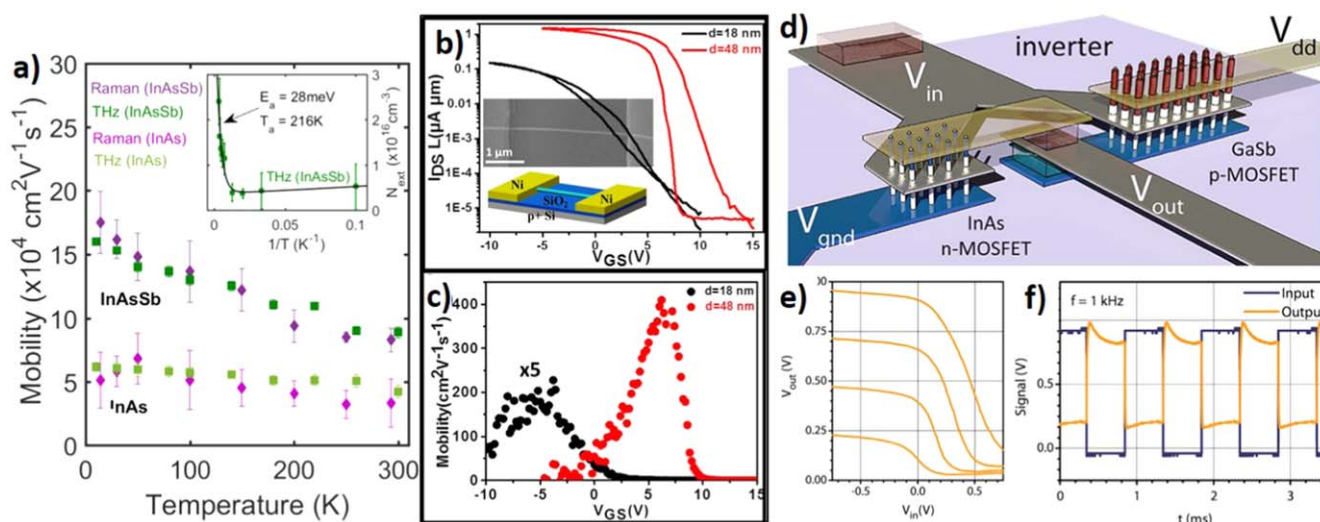


Figure 7. (a) Temperature dependent mobility of InAs and InAs_{0.65}Sb_{0.35} NWs extracted from terahertz and Raman spectra. The inset shows the extrinsic carrier concentration of InAs_{0.65}Sb_{0.35} NWs extracted from terahertz measurements as a function of inverse temperature [16] (adapted with permission from [16]. Copyright 2018 American Chemical Society). (b) Transfer characteristics of two Au-grown GaSb NWs with different diameters. The insets show a SEM image of a NWFET (up) and schematic image of a NWFET (down) [155]. (c) The mobilities of the GaSb NWs shown in (b) [155] (adapted with permission from [155]. Copyright 2015 American Chemical Society). (d) A schematic image of an inverter constructed by an InAs and GaSb NWFET. The spacing layers are omitted. (e) Voltage transfer characteristics for a NW-based inverter with different supply voltages from 0.25–1 V (0.25 V per step). (f) AC characterization of the inverter circuit [156] (adapted with permission from [156]. Copyright 2015 American Chemical Society).

fabricated in a NW heterojunction. Here, the III-Sb NW for a FET application is discussed.

5.1.1. n-type FET. Bulk InSb has the highest reported electron mobility among the III–V semiconductors. In a report by Gül *et al* [152], after optimization of several factors like long time evacuation, substrate cleaning and contact spacing, n-type InSb NWFETs with an average low temperature ($\sim 4.2 \text{ K}$) field-effect mobility of $\sim 2.5 \times 10^4 \text{ cm}^2 \text{ V}^{-1} \text{ s}^{-1}$ were obtained. The authors also demonstrated good reproducibility of these InSb NWFETs after process optimization.

Apart from computation, InSb FETs have been put in different applications. For example, InSb NWs were used to fabricate a NO₂ sensor [149]. The existence of NO₂ reduces the conductance of the InSb NW which makes the sensing possible. The NO₂ sensor is capable of sensing the NO₂ concentration up to one part-per-million (ppm). In another report, an InAs/InSb axial junction FET has been used for terahertz detection [32].

Using terahertz spectroscopy and the Raman spectroscopy technique, the InAs_{0.65}Sb_{0.35} NW was found to have high electron mobility ($\sim 16\,000 \text{ cm}^2 \text{ V}^{-1} \text{ s}^{-1}$) which makes it another potential candidate for high-performance electronics (figure 7(a)) [16].

One drawback of using low bandgap III-Sb NWs as n-channel devices is the enhancement of leakage current which still needs to be improved.

5.1.2. p-type FET. The development of a p-type antimonide-based NWFET is also important. However, development of a p-type III–V NWFET is challenging as the intrinsic NW always has an electron-rich surface layer which pins the Fermi

level in the conduction band. Therefore, p-doping of InAs and InSb becomes difficult. An *ex situ* Zn-doped process has been developed for an InAs NW and the device shows a peak hole mobility of $\sim 60 \text{ cm}^2 \text{ V}^{-1} \text{ s}^{-1}$ [153]. Yang *et al* developed an *in situ* carbon-doped p-type InSb NWFET that had field-effect mobility $\sim 140 \text{ cm}^2 \text{ V}^{-1} \text{ s}^{-1}$ [154].

As the fabrication of p-type GaSb and GaInSb NW becomes more mature, several high-performance p-NWFET reports have been published. Using sulfur surfactant-assisted growth, a Au-catalyzed GaSb NW with a diameter down to 16 nm was fabricated [155]. Fabricating them into back-gated NWFETs, peak hole mobility $\sim 400 \text{ cm}^2 \text{ V}^{-1} \text{ s}^{-1}$ was achieved with a hole concentration of $\sim 2.2 \times 10^{18} \text{ cm}^{-3}$ (figures 7(b) and (c)).

In another report, a NW-like GaSb structure of 20 nm in thickness was fabricated on a silicon substrate with the confinement of the SiO₂ shell achieved by using TASE [62]. Using complementary Hall measurements, the sheet carrier concentration of a GaSb sheet fabricated by TASE was extracted to be $2.4 \times 10^{17} \text{ cm}^{-2}$ with an average hole mobility of $760 \text{ cm}^2 \text{ V}^{-1} \text{ s}^{-1}$ which is close to bulk epitaxial GaSb films. In the same report, the authors also show that using TASE, a GaSb NW can be grown with an InAs NW with a controlled position and dimension on the same Si substrate without the InAs devices being affected. TASE provides a promising method to directly integrate all III–V CMOS on silicon for next-generation high-performance low-power electronics [62].

Reports have investigated the performance of all III–V NW CMOS with a GaSb NWFET as the p-channel (figure 7(d)). Some fundamental logic gate-like inverter (figures 7(e) and (f)) and NOT-AND (NAND) gates were demonstrated [156]. In a recent report, a self-aligned gate-last

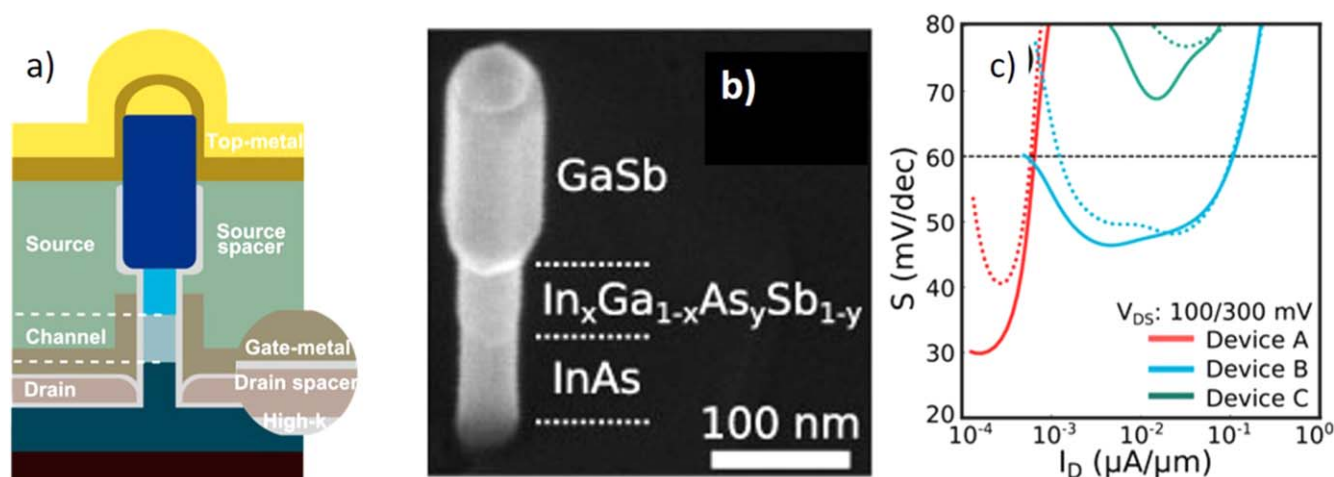


Figure 8. (a) Schematic diagram of a vertical InAs/InGaAsSb/GaSb NWFET [166] (adapted with permission from [166]. Copyright 2017 American Chemical Society). (b) SEM image of InAs/InGaAsSb/GaSb NW after growth. (c) Subthreshold slope versus drain current for a TFET with a different source doping level. Device A has a higher source doping level [30] (reproduced from [30]. © IOP Publishing Ltd. All rights reserved).

process was developed to co-integrate InAs and GaSb NWs into an all III–V CMOS on Si [157]. Although the performance of an InAs NWFET is improved through complex fabrication processes, further optimization is needed to balance the n-channel and p-channel for future all III–V CMOS integration.

5.1.3. TFET. A TFET is a promising device structure that allows the FET device to work below the thermionic limit (usually referred to as 60 mV/dec) of traditional metal-oxide-semiconductor field-effect transistor (MOSFETs) [158]. The motivation for developing this type of device is to fabricate ultra-low-power integrated circuits. A TFET is constructed by a p–n (or p–i–n) junction. Based on the charge carriers, the TFET can be a p- or n-type just like the MOSFET. The detailed working mechanism is presented in [159]. In brief, for a n-type TFET, at zero gate bias, the valence band of the p-junction and the conduction band of the n-junction are not aligned, and only very low current is passed through. The device is said to be OFF. With a positive gate voltage applied, the n-junction valence band and the p-junction conduction band overlap with each other. Charge carriers within a certain energy window can tunnel through the barriers.

Developing a NW TFET provides several advantages. For example, the implementation of a GAA structure provides good electrostatic control. Also, as the fabrication technique becomes more mature, materials with a wide range of possibilities (like diameter and composition) can be fabricated in a NW heterojunction. Antimonide-based NWs have been integrated into a TFET as both n-junction (e.g. InAsSb) and p-junction (e.g. GaSb) due to their low channel effective mass. A GaSb/InAs NW-based junction is the most studied system. The band structure of the junction can either be broken or staggered. One important feature of this junction is the high on-current due to the low channel effective mass [160, 161]. Fabricating a high-performance TFET that can work below the thermionic limit and exhibits a high

ON-current at the same time is challenging and needs a lot of optimization. For example, using the abovementioned TASE method, an InAs/GaSb n-TFET was fabricated [162]. The device showed a large subthreshold swing (1.4 V/dec) which might be due to the lack of intentional doping in the GaSb and the non-optimized gate stack suggested by the authors. In another report, an InAs/GaSb NW axial junction-based TFET with a 25 nm thick GaInAs insert integrated into a high-k top-gated configuration and showed a subthreshold swing of 350 mV/dec at $V_D = 100$ mV [163].

In recent years, Memisevic *et al* published a series of reports on a vertical InAs/GaSb NW-based TFET towards state-of-the-art performance. The reported NW junctions were fabricated on a highly n-doped InAs layer by MOVPE using a predefined Au catalyst. In 2016, a highly scaled InAs/GaSb NW TFET was fabricated utilizing a GAA geometry to improve electrostatic control [164]. The best device showed a subthreshold swing of 68 mV/dec which is still above the thermionic limit. The device also showed a high on-current $35 \mu\text{A} \mu\text{m}^{-1}$ at $V_{GS} = 0.5$ V and $V_{DS} = 0.5$ V. Later that year, the same group reported a NW TFET based on an InAs/GaSb NW TFET [165]. The device exhibited an improved below-thermionic subthreshold swing (48 mV/dec) for $V_{DS} = 0.1$ – 0.5 V, with an on-current of $10.6 \mu\text{A} \mu\text{m}^{-1}$ and off-current of $1 \text{ nA} \mu\text{m}^{-1}$ at $V_{DS} = 0.3$ V and with high I_{60} (the current when the subthreshold swing is 60 mV/dec). In 2017, they reported on an InAs/ $\text{In}_x\text{Ga}_{1-x}\text{As}_y\text{Sb}_{1-y}$ /GaSb vertical NW TFET with similar performance (figure 8(a)) [166]. Both devices presented a much higher current than the reported Si-based TFETs. Further study of source doping reduced the subthreshold swing to 30 mV/dec (figures 8(b)–(c)) [30]. This series of reports show that the performance of a TFET can be improved by (i) better electrostatic control with better gate stack, (ii) composition engineering of the junctions and (iii) optimized source doping. Further improvement might still be possible.

5.2. Optoelectronic applications

5.2.1. Light emitters. Light emitters based on a NW structure have several advantages. First of all, the good strain relaxation of the NW reduces the defects formed between the epilayers and growth substrates if the lattice parameter or thermal expansion coefficient do not match. These defects act as non-radiative scattering centers and lower the internal quantum efficiency (IQE) of the light emitter. The 1D structure of the NW enhances the light extraction and allows the photons to escape more easily. The bandgap of III–V materials covers from mid-IR to visible light to the UV spectrum. Their direct bandgap made them promising candidates for light emitters. III–N, III–P and also III–As based NWs are particularly well studied for LED and NW laser applications [167].

The studies into III–Sb NWs for light emitters are currently rather lacking, but they still have important applications—for example, LEDs and lasers that cover the mid-IR range of 2 μm to 5 μm are important in medical, gas sensor and materials processing.

GaSb-based NWs have been studied for potential NW laser applications. In 2006, the near-IR lasing properties of GaSb subwavelength wires with a cross-sectional dimension of 700–1500 nm were studied [168]. After that, antimonite-based NW has not been much studied. In recent years, Yuan *et al* demonstrated the potential of the spontaneous emission of NW based on a $\text{GaAs}_{1-x}\text{Sb}_x/\text{Al}_{1-y}\text{Ga}_y\text{As}$ radial quantum well (figure 9(a)) [84]. The radial growth behavior of $\text{GaAs}_{1-x}\text{Sb}_x$ was studied using MOVPE. The optimized $\text{GaAs}_{0.89}\text{Sb}_{0.11}/\text{Al}_{1-y}\text{Ga}_y\text{As}$ quantum well (QW) structure grown around the GaAs core was studied. The NWs showed strong PL emission around 903 nm at room temperature with a carrier lifetime of 305 ps. The IQE was also high at low excitation power which proved the QW structure had a high crystal quality after growth optimization. Combined with the Fabry–Perot cavity in the NW, strong amplified spontaneous emission was observed at both ends of the NW (810 to 930 nm) (figures 9(b) and (c)).

In another report [31], single-mode near-IR lasing (from 890 to 990 nm) was demonstrated on a single GaAs-based superlattice NW at room temperature (figures 9(d)–(e)). The GaAs NWs with GaAsSb inserts were grown using MBE. The GaAsSb inserts acted as a gain medium. With composition tuning, the lasing emission could be tuned from 890 to 990 nm (figure 9(f)). The superlattice structure demonstrated a low lasing threshold. The structure also had a high Q factor and high characteristic temperature. The unique superlattice structure provided a new design concept for a next-generation nanophotonic light source.

There is no III–Sb-based NW LED that has IR emission thus far. There is one report that used dilute-antimonite III–nitride NWs to realize a dot-in-wire LED [169]. The role of Sb here was to adjust the bandgap. With the incorporation of Sb (<1%), the bandgap of the GaN NW was tuned from 3.4 eV to ~ 2 eV due to the strong interaction between Ga and N-neighbors. By tuning the Sb incorporation, the emission wavelengths of the GaSbN/GaN tunnel junction LED could

be tuned from ~ 365 nm to 600 nm at room temperature. The LED also showed stable emission under injection current from 10 mA to 200 mA.

5.2.2. Photodetector. High carrier mobility and the direct bandgap of the III–Sb NW makes it a promising candidate for a high-performance photodetector. High carrier mobility leads to a low transit time which increases the gain. Particularly, as the bandgap of most III–Sb materials lies in the IR range, it is of utmost interest to develop a III–Sb NW-based IR detector.

Single junction field-effect type InSb [170, 171] and GaAsSb [172, 173] NW-based photodetectors were reported. Among them, an electrochemically fabricated InSb NWs-based photodetector shows very good responsivity ($8.4 \times 10 \text{ AW}^{-1}$) and quantum efficiency ($1.96 \times 10^6\%$) for an incident wavelength of 5.5 μm and power of 0.49 mW cm^{-2} [170]. The authors attributed the high responsivity and quantum efficiency to the high crystal quality, the high-aspect ratio of the NW structure and the enhanced space charge effect by the Schottky contacts formation. A CVD-grown $\text{GaAs}_{0.26}\text{Sb}_{0.74}$ NW-based photodetector shows a wide detection range from 1.16 μm to 1.55 μm with good responsivity and quantum efficiency [172].

With the maturation of the growth process of a III–Sb-based radial and axial heterostructure, a NW photodetector with improved device characteristics can be fabricated. For example, the shell layer can passivate the surface state of the NW core in a core–shell NW which increases the efficiency of NW devices [174, 175]. A room temperature IR photodetector based on an InAs/AlSb core–shell NW was reported recently. The AlSb shell layer provided good surface passivation and quantum confinement to the InAs NW (figure 10(a)) [13]. The phototransistor showed negative photoconductivity. Compared with a bare InAs NW phototransistor, the dark current was two orders of magnitude lower with a much-improved signal-to-noise ratio.

Ma *et al* fabricated Au-catalyzed GaSb/GaInSb p–n heterojunction NW using CVD (figure 10(b)) [176]. The GaSb and GaInSb junction formed a kinked angle due to the change in growth direction during GaInSb junction growth transits from GaSb. The crystal quality of the NWs was good. The device showed excellent quantum efficiency, responsivity and a short response time in the optical communication range.

A mid-IR photodetector has been demonstrated by using InAsSb/InAs NWs on different substrates [177–179]. The cutoff wavelength of the photodetector was found to be diameter dependent. The maximum 20% cutoff could reach 5.7 μm at 5 K for InAsSb with a diameter of 717 nm. The simulation result showed a higher cutoff could be obtained by enlarging the NW diameter.

In the report of Thompson *et al* the leakage current of the photodetector was reduced by a p–i–n junction (figures 10(c) and (d)) [177]. Their photodetector was constructed by a vertical p–i–n InAsSb NW array on InAs stems on the Si substrate. The photodetector showed a very low leakage current compared with a conventional InAs photodiode at

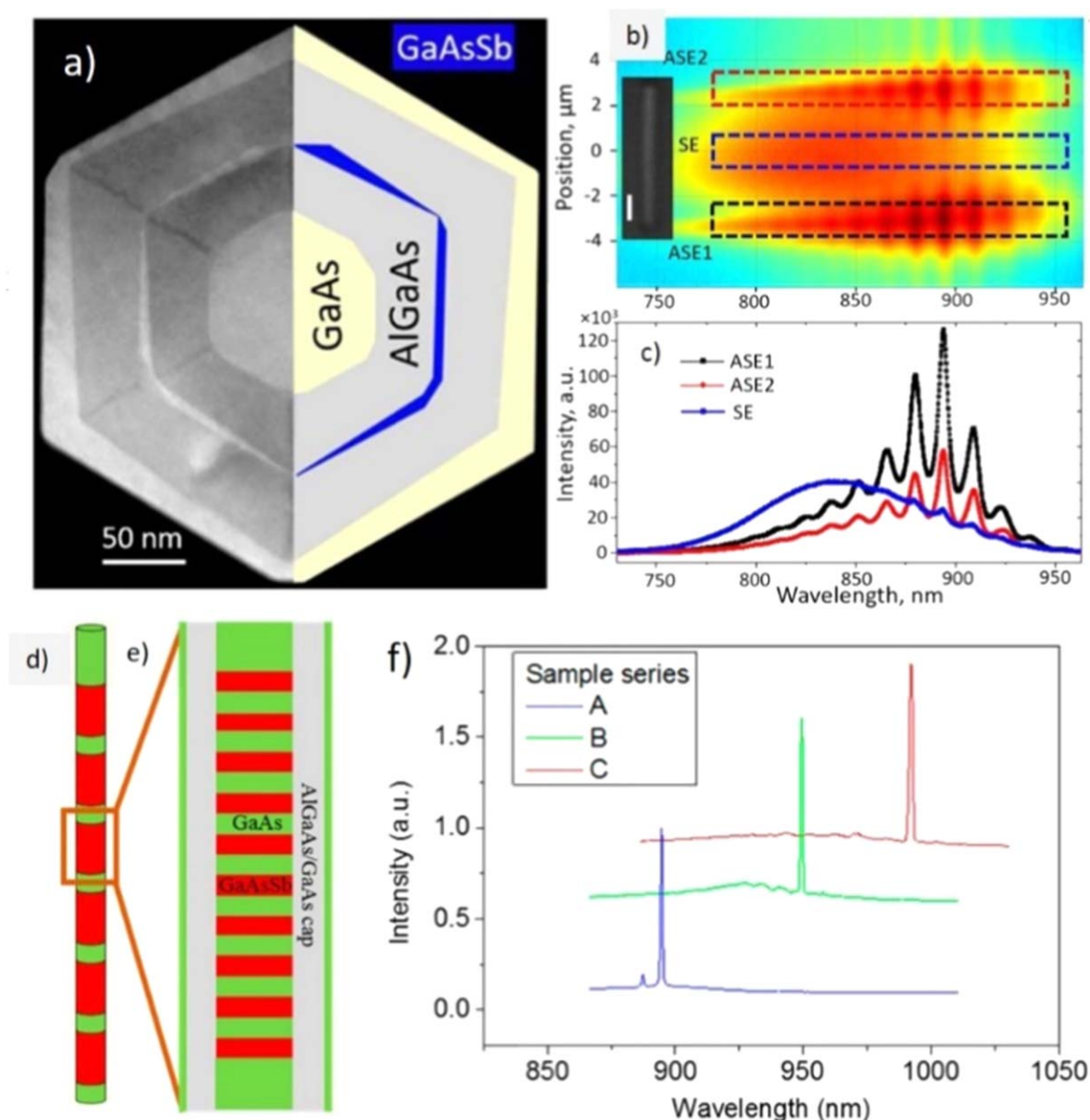


Figure 9. (a) Cross-sectional high-angle annular dark-field scanning transmission electron microscopy (HAADF-STEM) image of a GaAs/GaAs_{0.89}Sb_{0.11} QW NW [84]. (b) 1D hyperspectral map of a QW NW [84]. The NW in the inset illustrates the position. (c) Corresponding emission spectra of different positions in (b) [84] (adapted with permission from [84]. Copyright 2017 American Chemical Society). (d) and (e) Schematic image of the GaAsSb-based NW superlattice. (f) Lasing emission spectra of the NW with different Sb content profile. Sample A has the lowest Sb level (~ 1 at%) while Sample C has the highest (~ 8 at. %) [31] (adapted with permission from [31]. Copyright 2018 American Chemical Society).

room temperature [180]. An InAs NW-based photodetector is known to have high leakage current through the surface due to the existence of an electron accumulation layer which is also temperature dependent [180]. The authors attributed the low leakage current to good crystal quality and the absence of threading defects in the NWs.

So far, the antimonite-based photodetectors have shown good responsivity and good performance in near-IR to mid-IR sensing. The photodetectors have been in single junction type and axial heterojunction type in a single horizontal NW or vertical NW array. Study of a core-shell heterojunction-based NW photodetector is still lacking at this stage.

6. Outlook and conclusion

In summary, we have reviewed the recent advances of III-Sb NWs in terms of their synthesis and applications. As an important class of materials that has potential applications in high-performance electronics, optoelectronics and quantum computation, advances in crystal, morphology and composition engineering open up the opportunity of application development. As the surfactant role of the Sb is better understood, a new growth method can be developed to overcome the difficulty of growing high-quality III-Sb NWs in a more controllable manner.

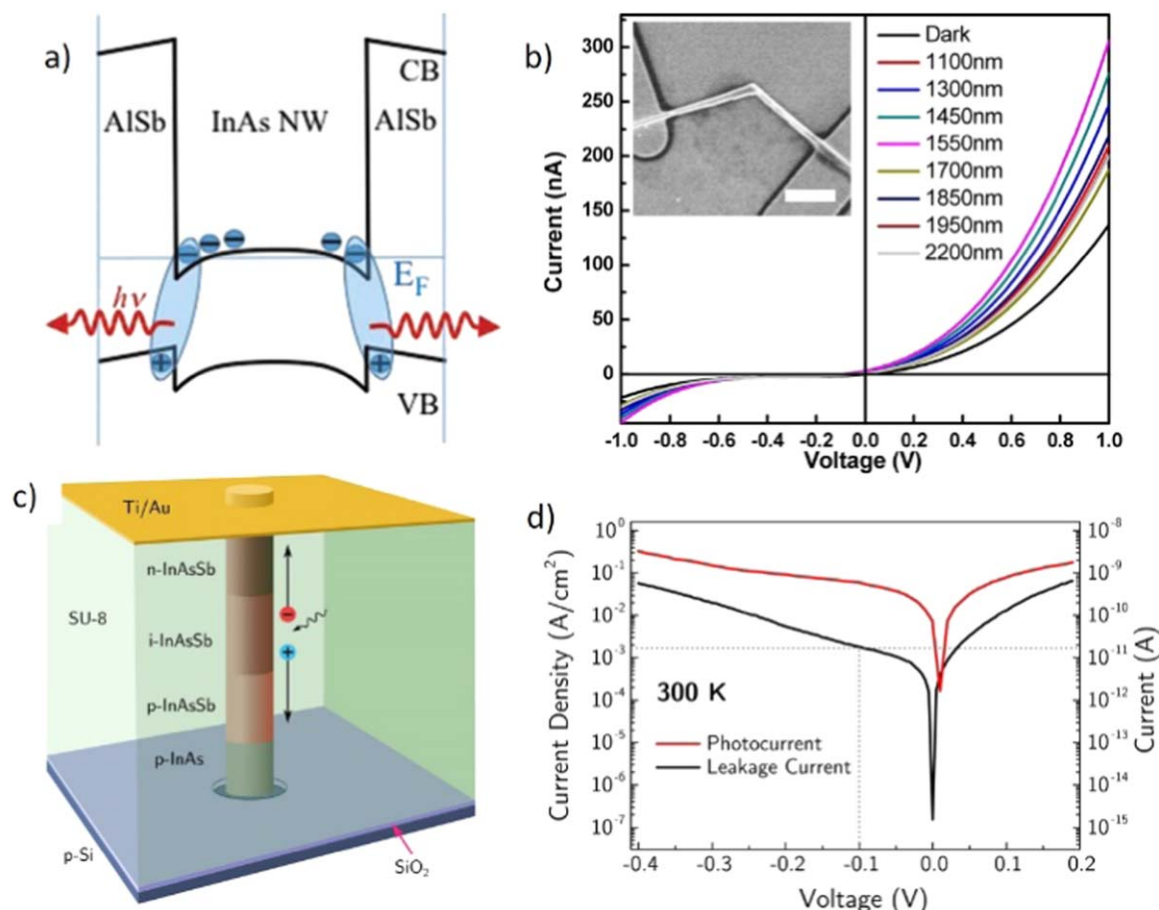


Figure 10. (a) Sketch of band bending of InAs/AISb core-shell NW [13] (John Wiley & Sons. © 2018 WILEY-VCH Verlag GmbH & Co. KGaA, Weinheim). (b) I-V characteristics of a single GaSb/Ga_{0.9}In_{0.1}Sb NW illuminated with a different wavelength under the same power. The insets represent the corresponding device [176] (adapted with permission from [176]. Copyright 2014 American Chemical Society). (c) Schematic of an InAsSb NW p-i-n junction photodiode [177]. (d) I-V characteristics of an InAs_{0.93}Sb_{0.07} p-i-n photodiode at 300 K [177] (adapted from [177]. CC BY 4.0).

In terms of further development of III-Sb NWs, we expect that the development of ternary and quaternary alloys will attract more attention as they offer one more degree to engineer the bandgap and the lattice constant, and hence the electrical and optical properties. Also, to engineer the properties of III-Sb NWs, Al-containing and N-containing III-Sb NWs might also attract considerable interest. Antimonides that contain these two elements are studied in their bulk form for various applications. Taking the mixed nitride-antimonide material system as an example, the interaction between nitrogen and antimony atoms allows a relatively large bandgap adjustment with a small amount of dopant (either N or Sb atoms) into the host lattice (antimonide). In section 5.2.1, with 1% of Sb incorporation into the GaN NWs, the bandgap is tuned from 3.4 eV to 2 eV. This is an important technique which provides one more degree of freedom to adjust the NW properties with better control in the lattice mismatch. In another system, III-V dilute nitride semiconductors—whereby a small amount of nitrogen atoms are incorporated into the III-V matrix—have been studied for optoelectronics [181] and solar cell applications [182, 183]. The advantage of this type of material is that with a few percents of nitrogen being incorporated into the III-V matrix, the bandgap can be effectively modulated; III-V dilute nitride semiconductors have therefore

been researched substantially in the bulk form. NW lasers based on GaAs/GaNAs core/shell structures have been demonstrated [184]. For III-Sb NWs, several attempts have been made to incorporate a few percents of nitrogen atoms into III-Sb NWs to form quaternary NW or shell layers [24, 185, 186]. After developing the material, creating the heterostructure is also important. So far, heterostructures with various material combinations have been fabricated. However, the development of complex heterostructures, such as the core-multishell configuration, is still lacking. These structures are extremely important in developing future optoelectronics.

Overall, III-Sb NW synthesis and their applications go hand-in-hand. As better NW fabrication methods are developed, more novel devices can also be obtained. Development is still lacking, especially for III-Sb NW-based optoelectronics, but we expect it will be developed rapidly in the near future.

Acknowledgments

This research was financially supported by the General Research Fund (CityU 11204614) and the Theme-based Research Scheme (T42-103/16-N) of the Research Grants

Council of Hong Kong SAR, China, the National Natural Science Foundation of China (51672229), the Science Technology and Innovation Committee of Shenzhen Municipality (Grant JCYJ20170818095520778) and a grant from Shenzhen Research Institute, City University of Hong Kong.

ORCID iDs

Johnny C Ho  <https://orcid.org/0000-0003-3000-8794>

References

- [1] Bennett B R, Magno R, Boos J B, Kruppa W and Ancona M G 2005 Antimonide-based compound semiconductors for electronic devices: a review *Solid. State. Electron.* **49** 1875–95
- [2] del Alamo J A 2011 Nanometre-scale electronics with III–V compound semiconductors *Nature* **479** 317–23
- [3] Mokkapat S and Jagadish C 2009 III–V compound SC for optoelectronic devices *Mater. Today* **12** 22–32
- [4] Lutchyn R M, Bakkers E P A M, Kouwenhoven L P, Krogstrup P, Marcus C M and Oreg Y 2018 Majorana zero modes in superconductor–semiconductor heterostructures *Nat. Rev. Mater.* **3** 52–68
- [5] Liu C, Li Y and Zeng Y 2010 Progress in antimonide based III–V compound semiconductors and devices *Engineering* **02** 617–24
- [6] Wolf O, Campione S, Kim J and Brener I 2016 Spectral filtering using active metasurfaces compatible with narrow bandgap III–V infrared detectors *Opt. Express* **24** 21512–20
- [7] Shafa M, Akbar S, Gao L, Fakhar-e-Alam M and Wang Z M 2016 Indium antimonide nanowires: synthesis and properties *Nanoscale Res. Lett.* **11** 164
- [8] Mingo N 2004 Thermoelectric figure of merit and maximum power factor in III–V semiconductor nanowires *Appl. Phys. Lett.* **84** 2652–4
- [9] Bennett B R, Ancona M G, Boos J B, Canedy C B and Khan S A 2008 Strained GaSb/AlAsSb quantum wells for p-channel field-effect transistors *J. Cryst. Growth* **311** 47–53
- [10] Lind E, Memisevic E, Dey A W and Wernersson L-E 2015 III–V heterostructure nanowire tunnel FETs *IEEE J. Electron Devices Soc.* **3** 96–102
- [11] Heida J P, van Wees B J, Kuipers J J, Klapwijk T M and Borghs G 1998 Spin-orbit interaction in a two-dimensional electron gas in a InAs/AlSb quantum well with gate-controlled electron density *Phys. Rev. B* **57** 11911–4
- [12] Tuttle G, Kroemer H and English J H 1989 Electron concentrations and mobilities in AlSb/InAs/AlSb quantum wells *J. Appl. Phys.* **65** 5239–42
- [13] Li H *et al* 2018 Novel Type-II InAs/AlSb core-shell nanowires and their enhanced negative photocurrent for efficient photodetection *Adv. Funct. Mater.* **28** 1705382
- [14] Kindlund H, Zamani R R, Persson A R, Lehmann S, Wallenberg L R and Dick K A 2018 Kinetic engineering of wurtzite and zinc-blende AlSb shells on InAs nanowires *Nano Lett.* **18** 5775–81
- [15] Rieger T, Grützmacher D and Lepsa M I 2015 InAs nanowires with Al_xGa_{1-x}Sb shells for band alignment engineering *J. Cryst. Growth* **425** 80–4
- [16] Boland J L, Amaduzzi F, Sterzl S, Potts H, Herz L M, Fontcuberta i Morral A and Johnston M B 2018 High electron mobility and insights into temperature-dependent scattering mechanisms in InAsSb nanowires *Nano Lett.* **18** 3703–10
- [17] Xia L, Boos J B, Bennett B R, Ancona M G and del Alamo J A 2011 Hole mobility enhancement in In_{0.41}Ga_{0.59}Sb quantum-well field-effect transistors *Appl. Phys. Lett.* **98** 053505
- [18] Gorji Ghalamestani S, Ek M, Ganjipour B, Thelander C, Johansson J, Caroff P and Dick K A 2012 Demonstration of defect-free and composition tunable Ga_xIn_{1-x}Sb Nanowires *Nano Lett.* **12** 4914–9
- [19] Ghalamestani S G, Ek M, Ghasemi M, Caroff P, Johansson J and Dick K A 2014 Morphology and composition controlled Ga_xIn_{1-x}Sb nanowires: understanding ternary antimonide growth *Nanoscale* **6** 1086–92
- [20] Zhou H, Pozuelo M, Hicks R F and Kodambaka S 2011 Self-catalyzed vapor–liquid–solid growth of InP_{1-x}Sb_x nanostructures *J. Cryst. Growth* **319** 25–30
- [21] Ngo C, Zhou H, Mecklenburg M, Pozuelo M, Regan B C, Xiao Q F, Shenoy V B, Hicks R F and Kodambaka S 2011 Effect of precursor flux on compositional evolution in InP_{1-x}Sb_x nanowires grown via self-catalyzed vapor–liquid–solid process *J. Cryst. Growth* **336** 14–9
- [22] Russell H B, Andriotis A N, Menon M, Jasinski J B, Martinez-Garcia A and Sunkara M K 2016 Direct band gap gallium antimony phosphide (GaSb_xP_{1-x}) Alloys *Sci. Rep.* **6** 20822
- [23] Xu Y, Liu R, Ma L, Li D, Yang Y, Dai G and Wan Q 2017 Fabrication of GaInPSb quaternary alloy nanowires and its room temperature electrical properties *Appl. Phys. A* **123** 6
- [24] Sharma M, Deshmukh P, Kasanaboina P, Reynolds C L, Liu Y and Iyer S 2017 Growth of defect-free GaAsSbN axial nanowires via self-catalyzed molecular beam epitaxy *Semicond. Sci. Technol.* **32** 125003
- [25] Chyi J - I, Biswas D, Iyer S V, Kumar N S, Morkoç H, Bean R, Zanio K, Lee H - Y and Chen H 1989 Molecular beam epitaxial growth and characterization of InSb on Si *Appl. Phys. Lett.* **54** 1016–8
- [26] Mori M, Murata K, Fujimoto N, Tatsuyama C and Tambo T 2007 Effect of AlSb buffer layer thickness on heteroepitaxial growth of InSb films on a Si(001) substrate *Thin Solid Films* **515** 7861–5
- [27] Mattias Borg B and Wernersson L-E 2013 Synthesis and properties of antimonide nanowires *Nanotechnology* **24** 202001
- [28] Caroff P, Messing M E, Mattias Borg B, Dick K A, Deppert K and Wernersson L-E 2009 InSb heterostructure nanowires: MOVPE growth under extreme lattice mismatch *Nanotechnology* **20** 495606
- [29] Ji X, Yang X and Yang T 2017 Self-catalyzed growth of vertical GaSb nanowires on InAs stems by metal-organic chemical vapor deposition *Nanoscale Res. Lett.* **12** 428
- [30] Memisevic E, Svensson J, Lind E and Wernersson L-E 2018 Impact of source doping on the performance of vertical InAs/InGaAsSb/GaSb nanowire tunneling field-effect transistors *Nanotechnology* **29** 435201
- [31] Ren D, Ahtapodov L, Nilsen J S, Yang J, Gustafsson A, Huh J, Conibeer G J, van Helvoort A T J, Fimland B-O and Weman H 2018 Single-mode near-infrared lasing in a GaAsSb-based nanowire superlattice at room temperature *Nano Lett.* **18** 2304–10
- [32] Pitanti A, Coquillat D, Ercolani D, Sorba L, Teppe F, Knap W, DeSimoni G, Beltram F, Tredicucci A and Vitiello M S 2012 Terahertz detection by heterostructured InAs/InSb nanowire based field effect transistors *Appl. Phys. Lett.* **101** 141103
- [33] Das S R, Delker C J, Zakharov D, Chen Y P, Sands T D and Janes D B 2011 Room temperature device performance of electrodeposited InSb nanowire field effect transistors *Appl. Phys. Lett.* **98** 243504

- [34] Hnida K, Mech J and Sulka G D 2013 Template-assisted electrodeposition of indium–antimony nanowires—comparison of electrochemical methods *Appl. Surf. Sci.* **287** 252–6
- [35] Park Y-S, Jung D H, Kim H J and Lee J S 2015 Annealed Au-assisted epitaxial growth of Si nanowires: control of alignment and density *Langmuir* **31** 4290–8
- [36] Han N, Wang F, Hou J J, Yip S, Lin H, Fang M, Xiu F, Shi X, Hung T and Ho J C 2012 Manipulated growth of GaAs nanowires: controllable crystal quality and growth orientations via a supersaturation-controlled engineering process *Cryst. Growth Des.* **12** 6243–9
- [37] Johansson J, Karlsson L S, Dick K A, Bolinsson J, Wacaser B A, Deppert K and Samuelson L 2009 Effects of supersaturation on the crystal structure of gold seeded III–V nanowires *Cryst. Growth Des.* **9** 766–73
- [38] Heo H *et al* 2012 Tunable catalytic alloying eliminates stacking faults in compound semiconductor nanowires *Nano Lett.* **12** 855–60
- [39] Han N, Wang Y, Yang Z, Yip S, Wang Z, Li D, Hung T F, Wang F, Chen Y and Ho J C 2017 Controllable III–V nanowire growth via catalyst epitaxy *J. Mater. Chem. C* **5** 4393–9
- [40] Tavendale A J and Pearton S J 1983 Deep level, quenched-in defects in silicon doped with gold, silver, iron, copper or nickel *J. Phys. C: Solid State Phys.* **16** 1665–73
- [41] Dick K A and Caroff P 2014 Metal-seeded growth of III–V semiconductor nanowires: towards gold-free synthesis *Nanoscale* **6** 3006–21
- [42] Tornberg M, Mårtensson E K, Zamani R R, Lehmann S, Dick K A and Ghalamestani S G 2016 Demonstration of Sn-seeded GaSb homo- and GaAs–GaSb heterostructural nanowires *Nanotechnology* **27** 175602
- [43] Zamani R R, Gorji Ghalamestani S, Niu J, Sköld N and Dick K A 2017 Polarity and growth directions in Sn-seeded GaSb nanowires *Nanoscale* **9** 3159–68
- [44] Yang Z *et al* 2017 Complementary metal oxide semiconductor-compatible, high-mobility, (111)-oriented GaSb nanowires enabled by vapor–solid–solid chemical vapor deposition *ACS Nano* **11** 4237–46
- [45] Qian Y and Yang Q 2017 Straight indium antimonide nanowires with twinning superlattices via a solution route *Nano Lett.* **17** 7183–90
- [46] Mandl B, Dick K A, Kriegner D, Keplinger M, Bauer G, Stangl J and Deppert K 2011 Crystal structure control in Au-free self-seeded InSb wire growth *Nanotechnology* **22** 145603
- [47] Sourribes M J L, Isakov I, Panfilova M, Liu H and Warburton P A 2014 Mobility enhancement by Sb-mediated minimisation of stacking fault density in InAs nanowires grown on silicon *Nano Lett.* **14** 1643–50
- [48] Anyebe E A and Zhuang Q 2014 Self-catalysed InAs_{1–x}Sb_x nanowires grown directly on bare Si substrates *Mater. Res. Bull.* **60** 572–5
- [49] Yu X, Li L, Wang H, Xiao J, Shen C, Pan D and Zhao J 2016 Two-step fabrication of self-catalyzed Ga-based semiconductor nanowires on Si by molecular-beam epitaxy *Nanoscale* **8** 10615–21
- [50] Li L *et al* 2017 Near full-composition-range high-quality GaAs_{1–x}Sb_x nanowires grown by molecular-beam epitaxy *Nano Lett.* **17** 622–30
- [51] Li L, Pan D, So H, Wang X, Yu Z and Zhao J 2017 GaAsSb/InAs core–shell nanowires grown by molecular-beam epitaxy *J. Alloys Compd.* **724** 659–65
- [52] Potts H, Morgan N P, Tütüncüoğlu G, Friedl M and Morral A F I 2017 Tuning growth direction of catalyst-free InAs(Sb) nanowires with indium droplets *Nanotechnology* **28** 054001
- [53] Lin A, Shapiro J N, Eisele H and Huffaker D L 2014 Tuning the Au-free InSb nanocrystal morphologies grown by patterned metal-organic chemical vapor deposition *Adv. Funct. Mater.* **24** 4311–6
- [54] Ji X, Yang X, Du W, Pan H and Yang T 2016 Selective-Area MOCVD growth and carrier-transport-type control of InAs (Sb)/GaSb core–shell nanowires *Nano Lett.* **16** 7580–7
- [55] Farrell A C, Lee W-J, Senanayake P, Haddad M A, Prikhodko S V and Huffaker D L 2015 High-quality InAsSb nanowires grown by catalyst-free selective-area metal-organic chemical vapor deposition *Nano Lett.* **15** 6614–9
- [56] Ren D *et al* 2016 New Insights into the origins of Sb-induced effects on self-catalyzed GaAsSb nanowire arrays *Nano Lett.* **16** 1201–9
- [57] Conesa-Boj S, Kriegner D, Han X-L, Plissard S, Wallart X, Stangl J, Fontcuberta i Morral A and Caroff P 2014 Gold-free ternary III–V antimonide nanowire arrays on silicon: twin-free down to the first bilayer *Nano Lett.* **14** 326–32
- [58] Fahed M, Desplanque L, Troadec D, Patriarche G and Wallart X 2016 Selective area heteroepitaxy of GaSb on GaAs (001) for in-plane InAs nanowire achievement *Nanotechnology* **27** 505301
- [59] Fahed M, Desplanque L, Troadec D, Patriarche G and Wallart X 2017 Threading dislocation free GaSb nanotemplates grown by selective molecular beam epitaxy on GaAs (001) for in-plane InAs nanowire integration *J. Cryst. Growth* **477** 45–9
- [60] Desplanque L, Bucamp A, Troadec D, Patriarche G and Wallart X 2018 In-plane InSb nanowires grown by selective area molecular beam epitaxy on semi-insulating substrate *Nanotechnology* **29** 305705
- [61] Schmid H, Borg M, Moselund K, Gignac L, Breslin C M, Bruley J, Cutaia D and Riel H 2015 Template-assisted selective epitaxy of III–V nanoscale devices for co-planar heterogeneous integration with Si *Appl. Phys. Lett.* **106** 233101
- [62] Borg M, Schmid H, Gooth J, Rossell M D, Cutaia D, Knoedler M, Bologna N, Wirths S, Moselund K E and Riel H 2017 High-mobility GaSb nanostructures cointegrated with InAs on Si *ACS Nano* **11** 2554–60
- [63] Tsuchida H, Nitta N, Yanagida Y, Okumura Y and Murase R 2018 Fibrous structure in GaSb surfaces irradiated with fast Cu cluster ions *J. Appl. Phys.* **123** 161548
- [64] Perez-Bergquist A G, Li K, Zhang Y and Wang L 2010 Ion irradiation-induced bimodal surface morphology changes in InSb *Nanotechnology* **21** 325602
- [65] Kluth S M, Llewellyn D and Ridgway M C 2006 Irradiation fluence dependent microstructural evolution of porous InSb *Nucl. Instruments Methods Phys. Res. Sect. B Beam Interact. with Mater. Atoms* **242** 640–2
- [66] Alkhaldi H S, Kluth P, Kremer F, Lysevych M, Li L, Ridgway M C and Williams J S 2017 Void evolution and porosity under arsenic ion irradiation in GaAs_{1–x}Sb_x alloys *J. Phys. D: Appl. Phys.* **50** 125101
- [67] Jany B R, Szajna K, Nikiel M, Wrana D, Trynkiewicz E, Pedrys R and Krok F 2015 Energy dependence of nanopillars formation on InSb semiconductor surfaces under gallium FIB and noble gas ions beam irradiation *Appl. Surf. Sci.* **327** 86–92
- [68] Kanamori Y, Kobayashi K, Yugami H and Hane K 2003 Subwavelength antireflection gratings for GaSb in visible and near-infrared wavelengths *Jpn. J. Appl. Phys.* **42** 4020–3
- [69] Razeghi M, Gin A, Wei Y, Bae J and Nah J 2003 Quantum sensing using Type II InAs/GaSb superlattice for infrared detection *Microelectronics J.* **34** 405–10
- [70] Lin T, Ramadurgam S, Liao C-S, Zi Y and Yang C 2015 Fabrication of Sub-25 nm diameter GaSb nanopillar arrays by nanoscale self-mask effect *Nano Lett.* **15** 4993–5000

- [71] Vardi A, Zhao X and del Alamo J A 2015 Quantum-size effects in sub 10-nm fin width InGaAs FinFETs 2015 *IEEE Int. Electron Devices Meeting (IEDM) (Piscataway, NJ)* (IEEE) pp 1–31
- [72] Zhou X *et al* 2016 Scalability of InGaAs gate-all-around FET integrated on 300 mm Si platform: demonstration of channel width down to 7 nm and Lg down to 36 nm 2016 *IEEE Symp. on VLSI Technology (Piscataway, NJ)* (IEEE) pp 1–2
- [73] Lu W, Zhao X, Choi D, ElKazzi S and del Alamo J A 2017 Alcohol-based digital etch for III–V vertical nanowires with Sub-10 nm diameter *IEEE Electron Device Lett.* **38** 548–51
- [74] Copel M, Reuter M C, Horn von Hoegen M and Tromp R M 1990 Influence of surfactants in Ge and Si epitaxy on Si(001) *Phys. Rev. B* **42** 11682–9
- [75] Portavoce A, Berbezier I and Ronda A 2003 Effect of Sb on Si/Si and Ge/Si growth process *Mater. Sci. Eng. B* **101** 181–5
- [76] Nimmatoori P, Zhang Q, Dickey E C and Redwing J M 2009 Suppression of the vapor–liquid–solid growth of silicon nanowires by antimony addition *Nanotechnology* **20** 025607
- [77] Du W-N, Yang X-G, Wang X-Y, Pan H-Y, Ji H-M, Luo S, Yang T and Wang Z-G 2014 The self-seeded growth of InAsSb nanowires on silicon by metal-organic vapor phase epitaxy *J. Cryst. Growth* **396** 33–7
- [78] Anyebe E A, Rajpalke M K, Veal T D, Jin C J, Wang Z M and Zhuang Q D 2015 Surfactant effect of antimony addition to the morphology of self-catalyzed InAs_{1-x}Sb_x nanowires *Nano Res.* **8** 1309–19
- [79] Dick K A, Caroff P, Bolinsson J, Messing M E, Johansson J, Deppert K, Wallenberg L R and Samuelson L 2010 Control of III–V nanowire crystal structure by growth parameter tuning *Semicond. Sci. Technol.* **25** 024009
- [80] Dheeraj D L, Patriarche G, Zhou H, Hoang T B, Moses A F, Grønsberg S, Van Helvoort A T J, Fimland B O and Weman H 2008 Growth and characterization of wurtzite GaAs nanowires with defect-free zinc blende GaAsSb inserts *Nano Lett.* **8** 4459–63
- [81] Xu T, Dick K A, Plissard S, Nguyen T H, Makoudi Y, Berthe M, Nys J-P, Wallart X, Grandidier B and Caroff P 2012 Faceting, composition and crystal phase evolution in III–V antimonide nanowire heterostructures revealed by combining microscopy techniques *Nanotechnology* **23** 095702
- [82] Zhuang Q D, Anyebe E A, Chen R, Liu H, Sanchez A M, Rajpalke M K, Veal T D, Wang Z M, Huang Y Z and Sun H D 2015 Sb-induced phase control of InAsSb nanowires grown by molecular beam epitaxy *Nano Lett.* **15** 1109–16
- [83] Yuan X, Caroff P, Wang F, Guo Y, Wang Y, Jackson H E, Smith L M, Tan H H and Jagadish C 2015 Antimony induced {112}A faceted triangular GaAs_{1-x}Sb_x/InP core/shell nanowires and their enhanced optical quality *Adv. Funct. Mater.* **25** 5300–8
- [84] Yuan X, Saxena D, Caroff P, Wang F, Lockrey M, Mokkapati S, Tan H H and Jagadish C 2017 Strong amplified spontaneous emission from high quality GaAs_{1-x}Sb_x single quantum well nanowires *J. Phys. Chem. C* **121** 8636–44
- [85] Jeppsson M, Dick K A, Wagner J B, Caroff P, Deppert K, Samuelson L and Wernersson L-E 2008 GaAs/GaSb nanowire heterostructures grown by MOVPE *J. Cryst. Growth* **310** 4115–21
- [86] Plissard S R, Slapak D R, Verheijen M A, Hoesvar M, Immink G W G, Van Weperen I, Nadj-Perge S, Frolov S M, Kouwenhoven L P and Bakkers E P A M 2012 From InSb nanowires to nanocubes: looking for the sweet spot *Nano Lett.* **12** 1794–8
- [87] Biefeld R M 2002 The metal-organic chemical vapor deposition and properties of III–V antimony-based semiconductor materials *Mater. Sci. Eng. R Reports* **36** 105–42
- [88] Caroff P, Wagner J B, Dick K A, Nilsson H A, Jeppsson M, Deppert K, Samuelson L, Wallenberg L R and Wernersson L 2008 High-quality InAs/InSb nanowire heterostructures grown by metal–organic vapor-phase epitaxy *Small* **4** 878–82
- [89] Ercolani D, Rossi F, Li A, Roddaro S, Grillo V, Salviati G, Beltram F and Sorba L 2009 InAs/InSb nanowire heterostructures grown by chemical beam epitaxy *Nanotechnology* **20** 505605
- [90] Dahl M, Namazi L, Zamani R R and Dick K A 2018 Sb Incorporation in wurtzite and zinc blende InAs_{1-x}Sb_x branches on InAs template nanowires *Small* **14** 1703785
- [91] Plissard S R *et al* 2013 Formation and electronic properties of InSb nanocrosses *Nat. Nanotechnol.* **8** 859–64
- [92] Lackner D *et al* 2009 Growth of InAsSb/InAs MQWs on GaSb for mid-IR photodetector applications *J. Cryst. Growth* **311** 3563–7
- [93] Lugani L, Ercolani D, Beltram F and Sorba L 2011 Growth mechanism of InAs-InSb heterostructured nanowires grown by chemical beam epitaxy *J. Cryst. Growth* **323** 304–6
- [94] Plissard S, Dick K A, Wallart X and Caroff P 2010 Gold-free GaAs/GaSb heterostructure nanowires grown on silicon *Appl. Phys. Lett.* **96** 121901
- [95] Dick K A, Thelander C, Samuelson L and Caroff P 2010 Crystal phase engineering in single InAs nanowires *Nano Lett.* **10** 3494–9
- [96] Ullah A R, Joyce H J, Burke A M, Wong-Leung J, Tan H H, Jagadish C and Micolich A P 2013 Electronic comparison of InAs wurtzite and zincblende phases using nanowire transistors *Phys. status solidi—Rapid Res. Lett.* **7** 911–4
- [97] Dayeh S A, Susac D, Kavanagh K L, Yu E T and Wang D 2009 Structural and room-temperature transport properties of zinc blende and wurtzite InAs nanowires *Adv. Funct. Mater.* **19** 2102–8
- [98] De A and Pryor C E 2010 Predicted band structures of III–V semiconductors in the wurtzite phase *Phys. Rev. B* **81** 155210
- [99] Fu M, Tang Z, Li X, Ning Z, Pan D, Zhao J, Wei X and Chen Q 2016 Crystal phase- and orientation-dependent electrical transport properties of InAs nanowires *Nano Lett.* **16** 2478–84
- [100] Yeh C-Y, Lu Z W, Froyen S and Zunger A 1992 Zinc-blende—wurtzite polytypism in semiconductors *Phys. Rev. B* **46** 10086
- [101] Ullah A R, Joyce H J, Tan H H, Jagadish C and Micolich A P 2017 The influence of atmosphere on the performance of pure-phase WZ and ZB InAs nanowire transistors *Nanotechnology* **28** 454001
- [102] Sestoft J E *et al* 2018 Engineering hybrid epitaxial InAsSb/Al nanowires for stronger topological protection *Phys. Rev. Mater.* **2** 044202
- [103] Lehmann S, Wallentin J, Jacobsson D, Deppert K and Dick K A 2013 A general approach for sharp crystal phase switching in InAs, GaAs, InP, and GaP nanowires using only group V flow *Nano Lett.* **13** 4099–105
- [104] Han N, Hou J J, Wang F, Yip S, Lin H, Fang M, Xiu F, Shi X, Hung T and Ho J C 2012 Large-scale and uniform preparation of pure-phase wurtzite GaAs NWs on non-crystalline substrates *Nanoscale Res. Lett.* **7** 632
- [105] Pan D *et al* 2014 Controlled synthesis of phase-pure InAs nanowires on Si(111) by diminishing the diameter to 10 nm *Nano Lett.* **14** 1214–20
- [106] Pozuelo M, Zhou H, Lin S, Lipman S A, Goorsky M S, Hicks R F and Kodambaka S 2011 Self-catalyzed growth of InP/InSb axial nanowire heterostructures *J. Cryst. Growth* **329** 6–11

- [107] Vogel A T, de Boor J, Becker M, Wittemann J V, Mensah S L, Werner P and Schmidt V 2011 Ag-assisted CBE growth of ordered InSb nanowire arrays *Nanotechnology* **22** 015605
- [108] Yang X, Wang G, Slattery P, Zhang J Z and Li Y 2010 Ultrasmall single-crystal indium antimonide nanowires *Cryst. Growth Des.* **10** 2479–82
- [109] Ghalamestani S G, Lehmann S and Dick K A 2016 Can antimonide-based nanowires form wurtzite crystal structure? *Nanoscale* **8** 2778–86
- [110] Thelander C, Caroff P, Plissard S and Dick K A 2012 Electrical properties of InAs_{1-x}Sb_x and InSb nanowires grown by molecular beam epitaxy *Appl. Phys. Lett.* **100** 232105
- [111] Namazi L, Gren L, Nilsson M, Garbrecht M, Thelander C, Zamani R R and Dick K A 2018 Realization of wurtzite GaSb using InAs nanowire templates *Adv. Funct. Mater.* **28** 1800512
- [112] Zhou C, Zheng K, Chen P-P, Matsumura S, Lu W and Zou J 2018 Crystal-phase control of GaAs–GaAsSb core–shell/axial nanowire heterostructures by a two-step growth method *J. Mater. Chem. C* **6** 6726–32
- [113] Nika D L, Cocemasov A I, Isacova C I, Balandin A A, Fomin V M and Schmidt O G 2012 Suppression of phonon heat conduction in cross-section-modulated nanowires *Phys. Rev. B* **85** 205439
- [114] Sansoz F 2011 Surface faceting dependence of thermal transport in silicon nanowires *Nano Lett.* **11** 5378–82
- [115] Algra R E, Verheijen M A, Borgström M T, Feiner L-F, Immink G, van Enckevort W J P, Vlieg E and Bakkers E P A M 2008 Twinning superlattices in indium phosphide nanowires *Nature* **456** 369–72
- [116] Suomalainen S, Hakkarainen T V, Salminen T, Koskinen R, Honkanen M, Luna E and Guina M 2015 Te-doping of self-catalyzed GaAs nanowires *Appl. Phys. Lett.* **107** 012101
- [117] Grap T, Rieger T, Blömers C, Schäpers T, Grützmacher D and Lepsa M I 2013 Self-catalyzed VLS grown InAs nanowires with twinning superlattices *Nanotechnology* **24** 335601
- [118] Yuan X, Guo Y, Caroff P, He J, Tan H H and Jagadish C 2017 Dopant-free twinning superlattice formation in InSb and InP nanowires *Phys. status solidi—Rapid Res. Lett.* **11** 1700310
- [119] Pea M, Ercolani D, Li A, Gemmi M, Rossi F, Beltram F and Sorba L 2013 Suppression of lateral growth in InAs/InAsSb heterostructured nanowires *J. Cryst. Growth* **366** 8–14
- [120] Ek M, Borg B M, Johansson J and Dick K A 2013 Diameter limitation in growth of III–Sb-containing nanowire heterostructures *ACS Nano* **7** 3668–75
- [121] Yang Z, Han N, Fang M, Lin H, Cheung H-Y, Yip S, Wang E-J, Hung T, Wong C-Y and Ho J C 2014 Surfactant-assisted chemical vapour deposition of high-performance small-diameter GaSb nanowires *Nat. Commun.* **5** 5249
- [122] Rudolph D, Schweickert L, Morkötter S, Loitsch B, Hertenberger S, Becker J, Bichler M, Abstreiter G, Finley J J and Koblmüller G 2014 Effect of interwire separation on growth kinetics and properties of site-selective GaAs nanowires *Appl. Phys. Lett.* **105** 033111
- [123] Gibson S J and LaPierre R R 2014 Model of patterned self-assisted nanowire growth *Nanotechnology* **25** 415304
- [124] Jensen L E, Björk M T, Jeppesen S, Persson A I, Ohlsson B J and Samuelson L 2004 Role of surface diffusion in chemical beam epitaxy of InAs nanowires *Nano Lett.* **4** 1961–4
- [125] Ren D, Huh J, Dheeraj D L, Weman H and Fimland B-O 2016 Influence of pitch on the morphology and luminescence properties of self-catalyzed GaAsSb nanowire arrays *Appl. Phys. Lett.* **109** 243102
- [126] Ercolani D, Gemmi M, Nasi L, Rossi F, Pea M, Li A, Salvati G, Beltram F and Sorba L 2012 Growth of InAs/InAsSb heterostructured nanowires *Nanotechnology* **23** 115606
- [127] Borg B M, Dick K A, Eymery J and Wernersson L-E 2011 Enhanced Sb incorporation in InAsSb nanowires grown by metalorganic vapor phase epitaxy *Appl. Phys. Lett.* **98** 113104
- [128] Namazi L, Ghalamestani S G, Lehmann S, Zamani R R and Dick K A 2017 Direct nucleation, morphology and compositional tuning of InAs_{1-x}Sb_x nanowires on InAs (111) B substrates *Nanotechnology* **28** 165601
- [129] Du W, Yang X, Pan H, Wang X, Ji H, Luo S, Ji X, Wang Z and Yang T 2015 Two different growth mechanisms for Au-free InAsSb nanowires growth on Si substrate *Cryst. Growth Des.* **15** 2413–8
- [130] Potts H, Friedl M, Amaduzzi F, Tang K, Tütüncüoğlu G, Matteini F, Alarcon Lladó E, McIntyre P C and Fontcuberta i Morral A 2016 From twinning to pure zincblende catalyst-free InAs(Sb) nanowires *Nano Lett.* **16** 637–43
- [131] Yuan X, Caroff P, Wong-Leung J, Tan H H and Jagadish C 2015 Controlling the morphology, composition and crystal structure in gold-seeded GaAs_{1-x}Sb_x nanowires *Nanoscale* **7** 4995–5003
- [132] Alarcón-Lladó E, Conesa-Boj S, Wallart X, Caroff P and Fontcuberta i Morral A 2013 Raman spectroscopy of self-catalyzed GaAs_{1-x}Sb_x nanowires grown on silicon *Nanotechnology* **24** 405707
- [133] Kang J-H, Cohen Y, Ronen Y, Heiblum M, Buczko R, Kacman P, Popovitz-Biro R and Shtrikman H 2013 Crystal structure and transport in merged InAs nanowires MBE grown on (001) InAs *Nano Lett.* **13** 5190–6
- [134] Rieger T, Rosenbach D, Vakulov D, Heedt S, Schäpers T, Grützmacher D and Lepsa M I 2016 Crystal phase transformation in self-assembled InAs nanowire junctions on patterned Si substrates *Nano Lett.* **16** 1933–41
- [135] Dalacu D, Kam A, Austing D G and Poole P J 2013 Droplet dynamics in controlled InAs nanowire interconnections *Nano Lett.* **13** 2676–81
- [136] Krizek F, Kanne T, Razmadze D, Johnson E, Nygård J, Marcus C M and Krogstrup P 2017 Growth of InAs wurtzite nanocrosses from hexagonal and cubic basis *Nano Lett.* **17** 6090–6
- [137] Car D, Wang J, Verheijen M A, Bakkers E P A M and Plissard S R 2014 Rationally designed single-crystalline nanowire networks *Adv. Mater.* **26** 4875–9
- [138] Gazibegovic S *et al* 2017 Epitaxy of advanced nanowire quantum devices *Nature* **548** 434–8
- [139] Rokhinson L P, Liu X and Furdyna J K 2012 The fractional a. c. Josephson effect in a semiconductor–superconductor nanowire as a signature of Majorana particles *Nat. Phys.* **8** 795–9
- [140] Das A, Ronen Y, Most Y, Oreg Y, Heiblum M and Shtrikman H 2012 Zero-bias peaks and splitting in an Al–InAs nanowire topological superconductor as a signature of Majorana fermions *Nat. Phys.* **8** 887–95
- [141] Deng M T, Yu C L, Huang G Y, Larsson M, Caroff P and Xu H Q 2012 Anomalous zero-bias conductance peak in a Nb–InSb nanowire–Nb hybrid device *Nano Lett.* **12** 6414–9
- [142] Stanescu T D, Lutchyn R M and Das Sarma S 2014 Soft superconducting gap in semiconductor-based Majorana nanowires *Phys. Rev. B* **90** 085302
- [143] Chen J, Yu P, Stenger J, Hocevar M, Car D, Plissard S R, Bakkers E P A M, Stanescu T D and Frolov S M 2017 Experimental phase diagram of zero-bias conductance peaks in semiconductor/semiconductor nanowire devices *Sci. Adv.* **3** e1701476

- [144] Gül Ö *et al* 2017 Hard superconducting gap in InSb nanowires *Nano Lett.* **17** 2690–6
- [145] Hasegawa H and Akazawa M 2008 Surface passivation technology for III–V semiconductor nanoelectronics *Appl. Surf. Sci.* **255** 628–32
- [146] Gül Ö *et al* 2018 Ballistic Majorana nanowire devices *Nat. Nanotechnol.* **13** 192–7
- [147] Gill S T, Damasco J, Janicek B E, Durkin M S, Humbert V, Gazibegovic S, Car D, Bakkers E P A M, Huang P Y and Mason N 2018 Selective-area superconductor epitaxy to ballistic semiconductor nanowires *Nano Lett.* **18** 6121–8
- [148] Webb J L, Knutsson J, Hjort M, Gorji Ghalamestani S, Dick K A, Timm R and Mikkelsen A 2015 Electrical and surface properties of InAs/InSb nanowires cleaned by atomic hydrogen *Nano Lett.* **15** 4865–75
- [149] Paul R K, Badhulika S and Mulchandani A 2011 Room temperature detection of NO₂ using InSb nanowire *Appl. Phys. Lett.* **99** 033103
- [150] Zhou F, Seol J H, Moore A L, Shi L, Ye Q L and Scheffler R 2006 One-dimensional electron transport and thermopower in an individual InSb nanowire *J. Phys. Condens. Matter* **18** 9651–7
- [151] Uryupin O N, Vedernikov M V, Shabaldin A A, Ivanov Y V, Kumzerov Y A and Fokin A V 2009 Thermoelectric properties of InSb nanowires over a wide temperature range *J. Electron. Mater.* **38** 990–3
- [152] Gül Ö, van Woerkom D J, van Weperen I, Car D, Plissard S R, Bakkers E P A M and Kouwenhoven L P 2015 Towards high mobility InSb nanowire devices *Nanotechnology* **26** 215202
- [153] Ford A C, Chuang S, Ho J C, Chueh Y L, Fan Z and Javey A 2010 Patterned p-doping of InAs nanowires by gas-phase surface diffusion of Zn *Nano Lett.* **10** 509–13
- [154] Yang Z, Han N, Wang F, Cheung H-Y, Shi X, Yip S, Hung T, Lee M H, Wong C-Y and Ho J C 2013 Carbon doping of InSb nanowires for high-performance p-channel field-effect transistors *Nanoscale* **5** 9671
- [155] Yang Z, Yip S, Li D, Han N, Dong G, Liang X, Shu L, Hung T F, Mo X and Ho J C 2015 Approaching the hole mobility limit of GaSb nanowires *ACS Nano* **9** 9268–75
- [156] Svensson J, Dey A W, Jacobsson D and Wernersson L-E 2015 III–V nanowire complementary metal–oxide semiconductor transistors monolithically integrated on Si *Nano Lett.* **15** 7898–904
- [157] Jonsson A, Svensson J and Wernersson L-E 2018 A self-aligned gate-last process applied to All-III–V CMOS on Si *IEEE Electron Device Lett.* **39** 935–8
- [158] Ionescu A M and Riel H 2011 Tunnel field-effect transistors as energy-efficient electronic switches *Nature* **479** 329–37
- [159] Convertino C, Zota C B, Schmid H, Ionescu A M and Moselund K E 2018 III–V heterostructure tunnel field-effect transistor *J. Phys. Condens. Matter* **30** 264005
- [160] Dey A W, Borg B M, Ganjipour B, Ek M, Dick K A, Lind E, Thelander C and Wernersson L-E 2013 High-current GaSb/InAs(Sb) nanowire tunnel field-effect transistors *IEEE Electron Device Lett.* **34** 211–3
- [161] Dey A W, Svensson J, Ek M, Lind E, Thelander C and Wernersson L-E 2013 Combining axial and radial nanowire heterostructures: radial esaki diodes and tunnel field-effect transistors *Nano Lett.* **13** 5919–24
- [162] Cutaia D, Moselund K E, Schmid H, Borg M, Olziersky A and Riel H 2016 Complementary III–V heterojunction lateral NW tunnel FET technology on Si 2016 *IEEE Symp. on VLSI Technology* (Piscataway, NJ: IEEE) pp 1–2
- [163] Borg B M, Dick K A, Ganjipour B, Pistol M-E, Wernersson L-E and Thelander C 2010 InAs/GaSb heterostructure nanowires for tunnel field-effect transistors *Nano Lett.* **10** 4080–5
- [164] Memisevic E, Svensson J, Hellenbrand M, Lind E and Wernersson L-E 2016 Scaling of vertical InAs–GaSb nanowire tunneling field-effect transistors on Si *IEEE Electron Device Lett.* **37** 549–52
- [165] Memisevic E, Svensson J, Hellenbrand M, Lind E and Wernersson L-E 2016 Vertical InAs/GaSb/GaSb tunneling field-effect transistor on Si with $S = 48 \text{ mV/decade}$ and $\text{Ion} = 10 \mu\text{A } \mu\text{m}^{-1}$ for $\text{Ioff} = 1 \text{ nA } \mu\text{m}^{-1}$ at $V_{\text{ds}} = 0.3 \text{ V}$ 2016 *IEEE Int. Electron Devices Meeting (IEDM)* (Piscataway, NJ: IEEE) pp 1–19
- [166] Memisevic E, Hellenbrand M, Lind E, Persson A R, Sant S, Schenk A, Svensson J, Wallenberg R and Wernersson L-E 2017 Individual defects in InAs/InGaAsSb/GaSb nanowire tunnel field-effect transistors operating below 60 mV/decade *Nano Lett.* **17** 4373–80
- [167] Zhang Y, Wu J, Aagesen M and Liu H 2015 III–V nanowires and nanowire optoelectronic devices *J. Phys. D: Appl. Phys.* **48** 463001
- [168] Chin A H, Vaddiraju S, Maslov A V, Ning C Z, Sunkara M K and Meyyappan M 2006 Near-infrared semiconductor subwavelength-wire lasers *Appl. Phys. Lett.* **88** 163115
- [169] Chowdhury F A, Sadaf S M, Shi Q, Chen Y-C, Guo H and Mi Z 2017 Optically active dilute-antimonide III-nitride nanostructures for optoelectronic devices *Appl. Phys. Lett.* **111** 061101
- [170] Kuo C-H H, Wu J-M M, Lin S-J J and Chang W-C C 2013 High sensitivity of middle-wavelength infrared photodetectors based on an individual InSb nanowire *Nanoscale Res. Lett.* **8** 327
- [171] Khan M I, Wang X, Jing X, Bozhilov K N and Ozkan C S 2009 Study of a single InSb nanowire fabricated via DC electrodeposition in porous templates *J. Nanosci. Nanotechnol.* **9** 2639–44
- [172] Ma L, Zhang X, Li H, Tan H, Yang Y, Xu Y, Hu W, Zhu X, Zhuang X and Pan A 2015 Bandgap-engineered GaAsSb alloy nanowires for near-infrared photodetection at $1.31 \mu\text{m}$ *Semicond. Sci. Technol.* **30** 105033
- [173] Li Z, Yuan X, Fu L, Peng K, Wang F, Fu X, Caroff P, White T P, Hoe Tan H and Jagadish C 2015 Room temperature GaAsSb single nanowire infrared photodetectors *Nanotechnology* **26** 445202
- [174] Mayer B *et al* 2013 Lasing from individual GaAs–AlGaAs core–shell nanowires up to room temperature *Nat. Commun.* **4** 2931
- [175] Mariani G, Zhou Z, Scofield A and Huffaker D L 2013 Direct-bandgap epitaxial core–multishell nanopillar photovoltaics featuring subwavelength optical concentrators *Nano Lett.* **13** 1632–7
- [176] Ma L *et al* 2014 Room-temperature near-infrared photodetectors based on single heterojunction nanowires *Nano Lett.* **14** 694–8
- [177] Thompson M D, Alhodaib A, Craig A P, Robson A, Aziz A, Krier A, Svensson J, Wernersson L-E, Sanchez A M and Marshall A R J 2016 Low leakage-current InAsSb nanowire photodetectors on silicon *Nano Lett.* **16** 182–7
- [178] Lee W-J, Senanayake P, Farrell A C, Lin A, Hung C-H and Huffaker D L 2016 High quantum efficiency nanopillar photodiodes overcoming the diffraction limit of light *Nano Lett.* **16** 199–204
- [179] Svensson J, Anttu N, Vainorius N, Borg B M and Wernersson L-E 2013 Diameter-dependent photocurrent in InAsSb nanowire infrared photodetectors *Nano Lett.* **13** 1380–5
- [180] Ker P J, Marshall A R J, Krysa A B, David J P R and Tan C H 2011 Temperature dependence of leakage current in InAs avalanche photodiodes *IEEE J. Quantum Electron.* **47** 1123–8
- [181] Harris J S 2002 GaInNAs long-wavelength lasers: progress and challenges *Semicond. Sci. Technol.* **17** 880–91

- [182] Geisz J F and Friedman D J 2002 III N V semiconductors for solar photovoltaic applications *Semicond. Sci. Technol.* **17** 769–77
- [183] Kim T W, Forghani K, Mawst L J, Kuech T F, La Lumondiere S D, Sin Y, Lotshaw W T and Moss S C 2014 Properties of ‘bulk’ GaAsSbN/GaAs for multi-junction solar cell application: reduction of carbon background concentration *J. Cryst. Growth* **393** 70–4
- [184] Chen S, Jansson M, Stehr J E, Huang Y, Ishikawa F, Chen W M and Buyanova I A 2017 Dilute nitride nanowire lasers based on a GaAs/GaNAs core/shell structure *Nano Lett.* **17** 1775–81
- [185] Kasanaboina P K, Ahmad E, Li J, Reynolds C L, Liu Y and Iyer S 2015 Self-catalyzed growth of dilute nitride GaAs/GaAsSbN/GaAs core-shell nanowires by molecular beam epitaxy *Appl. Phys. Lett.* **107** 103111
- [186] Kasanaboina P, Sharma M, Deshmukh P, Reynolds C L, Liu Y and Iyer S 2016 Effects of annealing on GaAs/GaAsSbN/GaAs core-multi-shell nanowires *Nanoscale Res. Lett.* **11** 47